TA7
C6
CER61-72
copy 2

B-76

FORCES AND MOMENTS ON A RESTRAINED MODEL IN REGULAR WAVES

ENGINEERING RESEARCH
SEP 27 '73
FOOTHILLS READING ROOM

by

E. F. Schulz

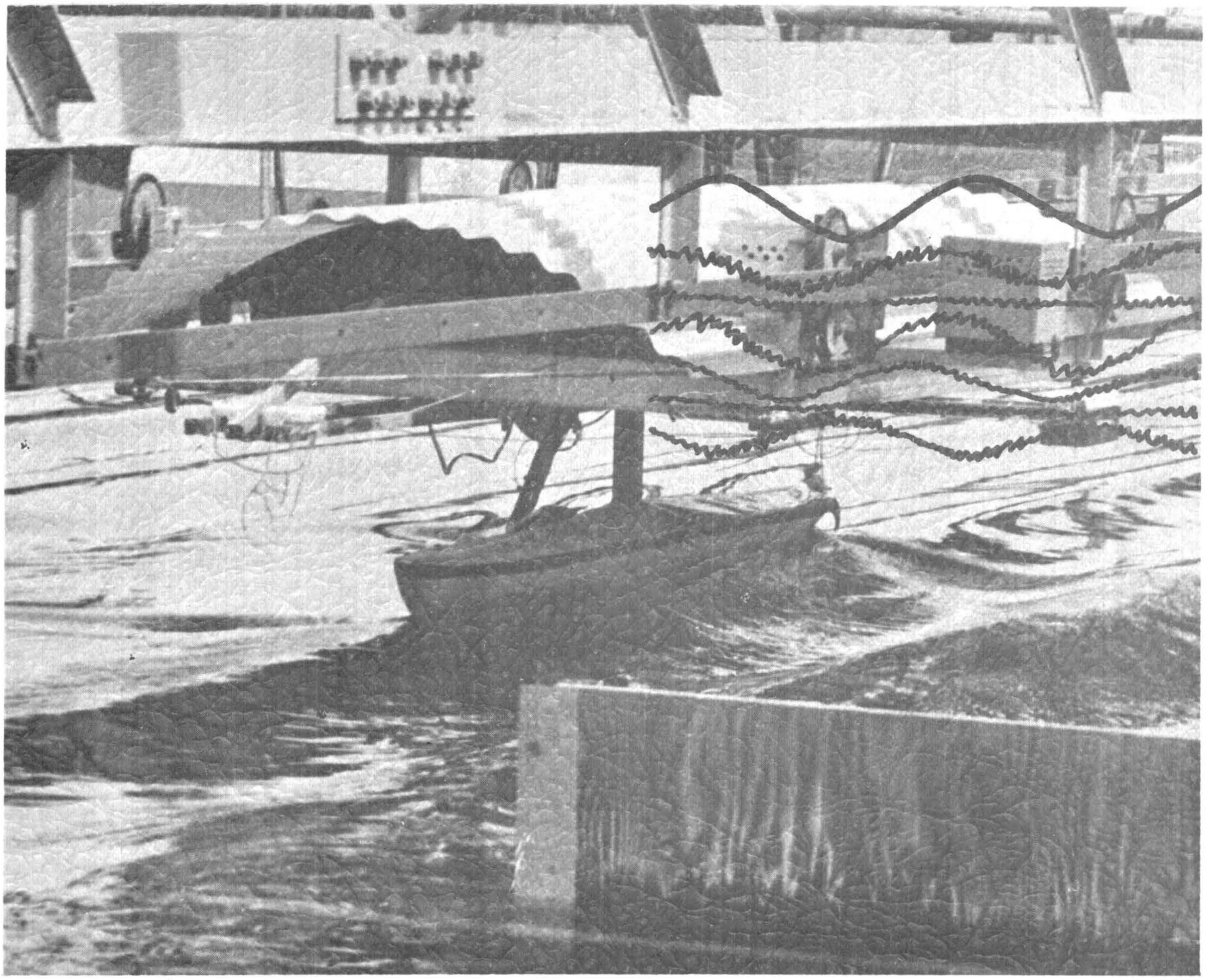

Prepared for David Taylor Model Basin
Department of the Navy, Under Contract Nonr 1610(04)
Through the
Colorado State University Research Foundation
Civil Engineering Section, Colorado State University
Fort Collins, Colorado

March 1961 CER61EFS72

Reproduction in whole or in part
is permitted for any purpose of
the United States Government.

FORCES AND MOMENTS ON A RESTRAINED MODEL IN REGULAR WAVES

by

E. F. Schulz

Civil Engineering Section
Colorado State University
Fort Collins, Colorado

Prepared for
David Taylor Model Basin
Department of the Navy
Under Contract Nonr 1610(04)

Through the

Colorado State University Research Foundation

March 1961 CER61EFS72

U18401 0593283

ABSTRACT

This report presents the experimental forces and moments acting on a five-foot model tanker when it was towed on five headings in a regular seaway. The seaway consisted of regular deep-water waves whose length varied from 0.5 to 2.0 times the model length. The wave steepness was varied from 1/40 to 1/20 height-length ratio. All motions of the model except uniform forward translation were restrained and the forces and moments relative to a moving towing carriage were measured with a six-component balance. The forces and moments were divided into steady-state and oscillatory forces and moments. The steady-state forces and moments are generally analogous to the forces and moments which would result if the model were towed in calm water. The oscillatory forces and moments are induced by the waves.

CONTENTS

TABLES

FIGURES

FIGURES - Continued

Figure No.

WAVE PROPERTIES

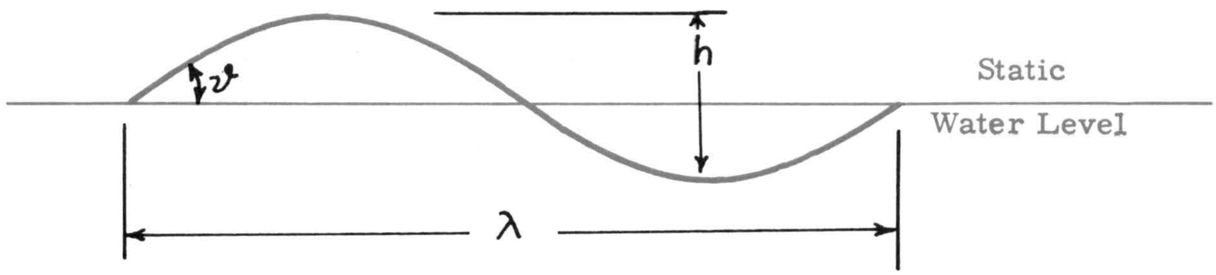

PRINCIPAL AXES OF SHIP

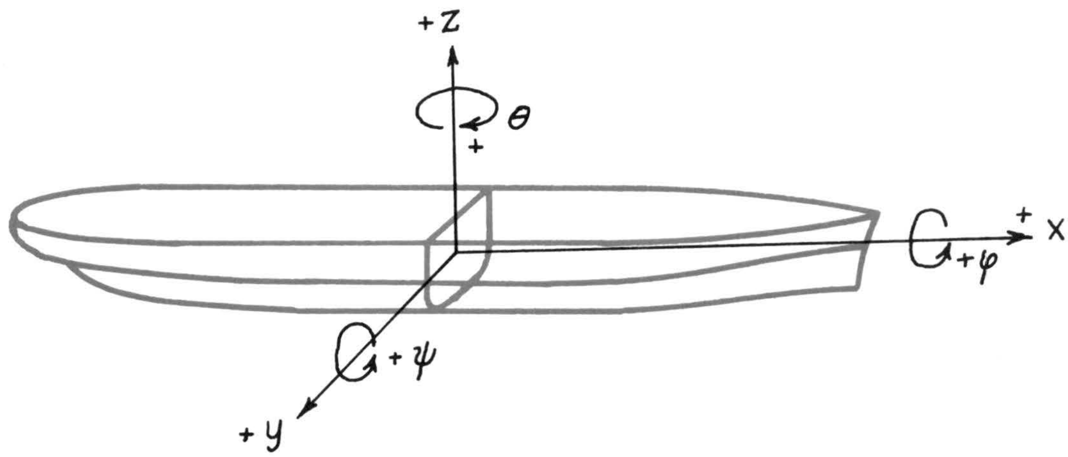

PROPERTIES OF THE SEAWAY

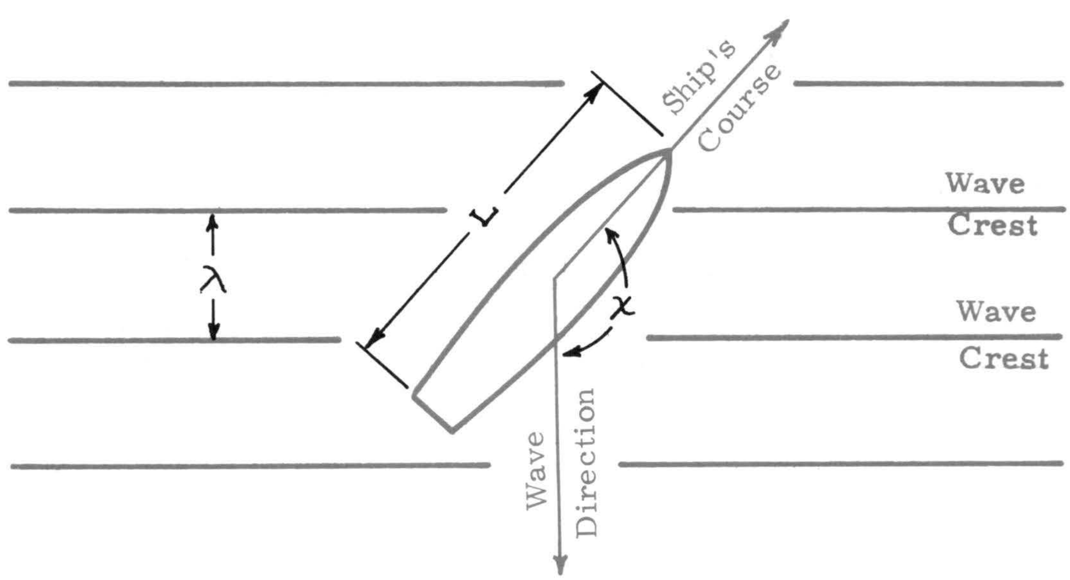

NOTATION

Symbol	Units	Definition
A_m	$(feet)^2$	Area of midship section
A_w	$(feet)^2$	Waterplane area
B	feet	Beam
c	feet/sec.	Wave celerity
C_B	----	Block coefficient $\frac{\nabla}{LBD}$
C_M	----	Maximum section coefficient
C_w	----	Waterplane coefficient, $\frac{A_w}{BL}$
d	feet	Depth of water
D	feet	Draft
Fr	----	Froude Number $v \sqrt{gL}$
F_x	pounds	Force in x direction
F_y	pounds	Force in y direction
F_z	pounds	Force in z direction
f	cps	Wave frequency
g	$feet/sec.^2$	Acceleration of gravity $32.16 ft/sec.^2$
h	feet	Wave height (double amplitude)
L	feet	Water line length
M_φ	inch-pounds	Rolling moment
M_ψ	inch-pounds	Pitching moment
M_θ	inch-pounds	Yawing moment

NOTATION-Continued

Symbol	Units	Definition
T_e	seconds	Period of encounter
v	feet/sec.	Speed of model
χ	degrees	Angle of heading of ship relative to direction of wave travel
λ	feet	Wave length
ϑ	degrees	Wave slope
ν	radius/sec.	Natural frequency
w	radius/sec.	Wave circular frequency
w_e	radius/sec.	Frequency of encounter
Δ	pounds	Displacement of model
∇	$(\text{feet})^3$	Volume of displacement

I. INTRODUCTION

The research work described in this report was conducted for the David Taylor Model Basin, Department of the Navy, under Contract Nonr 1610(04). Part of the tests in head seas were previously reported (1).

The experiments were conducted on a 5-foot model tanker. The same model was used in other experiments (1), (2), (3). The model was identified as Model "H" in resistance tests reported by Couch and St. Denis (3). The hull sections and lines are shown in reference (2), (3).

The normal motions of the model in response to the seaway were restrained. A six-component force balance, mounted in the model, engaged a rigid strut on the towing carriage. In this way the forces and moments acting on the model were measured with reference to the towing carriage. The towing carriage was towed at various uniform speeds, on different headings in a regular wave train.

II. METHOD AND PROCEDURE

The model used was a 5-foot tanker constructed from fiberglas-plastic laminate and reinforced with aluminum frames. The model particulars are shown in Table 1.

Six-Component Balance

The six-component balance previously used (1) was redesigned to increase the natural frequency of the flexural elements. The different flexural elements were machined from four two-inch cubes of magnesium, and one 2-inch by 2-inch by 6-inch block of magnesium. The design of the flexural elements was patterned after the modular force-blocks used by the David Taylor Model Basin in several force balances. The principal differences were that the force block was machined from a 2-inch cube instead of a 4- or 6-inch cube and was made from magnesium instead of steel or beryllium copper. These changes were made to give a reasonable signal for the size of the forces and moments involved. The six-component balance is shown in Fig. 1. The forward force unit is shown in greater detail in Fig. 2.

Electrical signals proportional to the forces experienced by the flexural elements are provided by Type C-19 SR-4 strain gages. The gages were connected as a Wheatstone bridge employing four active arms. The bridge output was amplified using a carrier-type amplifier system and recorded on a multichannel oscillograph.

The six-component force balance was mounted in the model so that the horizontal longitudinal axis was in the normal waterplane of the model. The longitudinal axis of the force balance was also positioned in vertical longitudinal plane of symmetry of the model. The vertical axis of the force balance was in the plane of the midship section of the model.

The force balance was calibrated by floating the model in a small calibration tank. The towing strut was clamped rigidly and the different forces and moments were individually applied to the model. Each force or moment was applied to model over a range of values in each direction. The positive direction or sense of each force and moment is shown on page vi .

Towing Carriage

The aluminum towing carriage is suspended from two carefully levelled and aligned rails. The rails were supported by a movable steel truss bridge spanning the wave basin. The carriage was attached to an endless steel cable. The towing cable was operated by a variable-speed electric D-C motor mounted at one end of the bridge. The motor speed was controlled by matching the actual motor speed measured by a tachometer against the speed set at the control. When an error between the actual speed and the specified speed developed, the armature current was automatically adjusted to correct the error.

The model speed was varied from zero to 3.17 feet per second which corresponded to a Froude number of 0 to 0.25.

Seaway

The model was towed on different headings in various regular wave systems. The wave length was varied from 2.4 feet to 9.4 feet which corresponded to λ/L values of 0.48 to 1.90.

The maximum wave steepness for the longer wave lengths was limited by the capability of the wave generator. The wave steepness was varied from 1/40 to 1/20 or from 1/40 to the capacity of the wave generator. Table 2 is a list of the various wave configurations to which the model was subjected on each heading.

The headings on which the model travelled varied from $\chi = 0^0$ to $\chi = 180^0$. The five different headings were achieved by moving the bridge around the basin periphery to the proper orientation in relation to the wave train. Figure 3 shows the bridge oriented to $\chi = 90^0$ and the travel of the model in beam seas. Figure 4 is another photograph of the model being towed in beam seas.

III. EXPERIMENTAL RESULTS

The forces and moments acting on the model during these experiments are the result of various actions on the model. Some of the forces are peculiar to this particular set of experiments; while others may be considered to be present in any model experiment. The forces and moments acting on the model are caused by:

1. acceleration of water in the vicinity of the model resulting from the general velocity field which is developed by the flow around the hull;
2. the hydrostatic and velocity fluctuations caused by the passage of waves;
3. skin friction resulting from flow over the surface of the hull;
4. the wave train created by the movement of the model through the water;
5. the vibration of the model supported by the force balance.

These forces and moments acting on the model may be further divided into three groups:

1. the steady-state forces and moments;
2. the oscillatory forces and moments;
3. the noise or spurious forces experienced by the model system.

Steady-State Forces and Moments

If the restrained model is towed in calm water, certain forces and moments result. These result from the steady flow pattern which is established by the movement of the model through the water and from the manner in which the model is attached to the six-component balance. These forces can also be recognized in the records of tests in waves by an apparent shift of the zero axis or zero line.

The existence of a positive heave force, a negative pitching moment and a negative drag force can be explained in this way. The direction sense of the forces and moments is shown in the diagram on page vi . The presence of steady-state forces on some headings in waves as recognized by the zero-shift is explained on the basis of waves which are reflected from one side of the model and not from the other side or by more effective reflection from the fore-body than from the after-body of the model.

Oscillatory Forces and Moments

The forces and moments acting on the model as a result of the waves will be time varying in nature. These are called oscillatory forces. The period of the oscillatory forces is equal to the period of encounter of the model. The oscillatory forces were superimposed on the steady state forces.

The ratio of the range in oscillatory force to the wave slope, ϑ , was used in previous report (1) in order to remove wave steepness as a variable from the wave geometry. Examination of the results shown in reference (1) shows that this was not entirely effective in eliminating the wave steepness as a variable. This is probably due to the fact that the wave reflection coefficient is also related to both the wave steepness and wave period. The data presented in this report are shown as simply the range in oscillatory force. The oscillatory forces and moments are shown in Figs. 5 to 40 as a function of the Froude number in parameters of wave length, λ/L , and wave steepness, h/λ .

Noise

The forces and moments acting on the model were measured by sensing the minute deflection of several relatively stiff springs. Since the model and carriage are a spring-mass system, the system is set in oscillation at its natural frequency by some disturbance. The natural frequency of a well designed transducer should be much higher than the frequency of the signal which one expects to measure. The disturbance setting the system in oscillation is the initial acceleration along the direction of travel when the run is started. The oscillation is sustained during the run by carriage vibration and by wave impact on the model. These spurious vibrations are called "noise" and are superimposed upon the record of steady-state force and the oscillatory forces previously discussed.

The design of the transducer is a compromise between a sufficient deflection to produce an adequate signal on one hand and enough stiffness to obtain a high natural frequency on the other hand. In order to obtain a readable signal, concessions had to be made in spring stiffness in the design of six-component balance. This resulted in a lower natural frequency and a higher noise-to-signal ratio. The balance used in this series of experiments had a lower noise-to-signal ratio than the one previously used and described in reference (1). It was still necessary to hand-fair the records in order to be able to obtain the data.

Heading Angle

The angle of heading was changed by changing the position of the towing bridge over the wave basin or by reversing the model on the carriage and beginning the test run from the other end of the towing bridge. The heading angle, χ , is shown on the definition sketch on page v and is defined as the vector angle between the direction of wave celerity, c , and direction of the ship velocity, v . Five different angles of heading were used during these experiments. They were:

$$\chi = 0^0,\ 45^0,\ 90^0,\ 135^0, \text{ and } 180^0 .$$

These headings are sometimes called: following seas, quartering seas, beam seas, quartering seas and head seas respectively.

The angle of heading is used in the computation of the Period of Encounter:

$$T_e = \frac{\lambda}{2.26\sqrt{\lambda} - v\cos\chi}$$

This equation shows that a set of runs having the same speed, v, and wave length, λ, will have a different period of encounter for each heading.

The reflection coefficient of the waves depends upon the angle with which the wave strikes the reflecting surface. Thus the reflection of waves from the model is different for each heading.

For these two reasons, the magnitude of the oscillatory forces and to some extent the steady-state forces would vary from heading to heading for each set of runs.

IV. DISCUSSION OF RESULTS

The data have been plotted on the respective graphs using distinctive symbols so that test runs having the same wave steepness and wave length can be identified. In most cases duplicate test runs were successfully completed. Many times the results were the same; in these cases the symbol representing two or more runs is slightly larger than the symbol size normally used.

Oscillatory Forces and Moments

The oscillatory forces and moments were plotted as a function of Froude number. The force or moment is shown as the range in force (double amplitude).

Heave Force

The oscillatory heave force was slightly speed dependent. For the longest wave length $\lambda/L \approx 2.0$, there was about a 10 percent reduction in heave force as the speed increased from $Fr = 0$ to $Fr = .25$. The shortest wave length $\lambda/L \approx 0.5$ showed little if any variation with speed. The greatest values of heave force were experienced in the longest wave length ($\lambda/L \approx 2.0$) on each heading.

The largest range in oscillatory heave force was found on the 45^0 heading (see Fig. 6) followed by the 0^0 heading (following seas). There were larger values of force where the apparent wave length was longest and there was greatest length of time for the model to experience the difference in hydrostatic buoyancy between the wave crest and the trough. At $\chi = 45^0$ the distance between succeeding crests was greatest hence the largest range in heave force. The range of heave force was greater in those cases where the period of encounter was greater, compare the values for $\chi = 45^0$ (Fig. 6) with $\chi = 135^0$ (Fig. 8) which are supplementary headings.

Larger values of heave force were also associated with the steeper waves or where the wave height was greatest. This is logical because here the difference in hydrostatic buoyancy between crest and trough is the greatest. Notice that any type symbol having a horizontal or downward spike on Figs. 5 to 9 has a larger value of heave force than the corresponding run not having the spike.

Pitching Moment

The oscillatory pitch moment was larger at the higher speeds where the Froude number, Fr , was .20 and .25 . There were two exceptions for the longer wave lengths $\lambda/L = 1.4$ and 1.9 and heading $\chi = 0^0$ where the range of pitching moment consistently decreased with increasing speed. During nearly all runs the range in pitching moment decreased when the speed was increased from 0 to $Fr = 0.5$ and then the range in pitching moment increased to the highest speed.

On any heading, the oscillatory pitching moment increased in range as the relative wave length increased until the waves were longer than the hull of the model; then the magnitude of the pitching moment was related to the actual wave height, h , rather than the relative wave length, λ/L . Notice on Fig. 11, how the values of pitching moment were similar for the runs where the wave height, h , was 0.25 feet.

The greatest range in pitching moment was found where $\chi = 0^0$ (following seas) and decreased to minimum values at $\chi = 90^0$ (beam seas) and then increased as the heading angle increased again to $\chi = 180^0$ (head seas). The pitching moment for the longer wave lengths on heading $\chi = 0^0$ was less than one-half the values on $\chi = 90^0$. (Compare Figs. 10 and 12.)

Rolling Moment

The influence of speed on the amplitude of the Oscillatory Rolling Moment was more complex than for the previous two cases. For the two headings, $\chi = 0^0$ and 180^0, the rolling moment decreased somewhat between $Fr = 0$ and 0.05 and increased to a maximum value at $Fr = .20$ or $.25$. On the oblique headings $\chi = 45^0$ and 135^0, the range of rolling moment was generally higher at the highest speeds. In a number of instances there was a small decrease between $Fr = 0$ and $.07$ before the rolling moment increased. On these headings the rolling moment was minimized at speeds corresponding to $Fr = .05$. On the $\chi = 90^0$ heading, the range in rolling moment decreased at the highest speeds. The relationship between speed and rolling moment for the low speeds was complex.

The oscillatory rolling moment was more related to wave height and wave steepness than to wave length. At zero speed it could be generally stated that the range in rolling moment was smallest for the shortest wave length and largest for the longest waves. This trend was reversed at the top speed on the 90^0 and 135^0 headings (see Figs. 17 and 18) where the range in rolling moment was largest for the shortest and steepest waves.

Sway Force

The variation of the sway force with increasing speed was shown on Figs. 20 through 24. There was no explanation for the presence of a sway force on the $\chi = 0^0$ and $\chi = 180^0$ headings (Figs. 20 and 24). The force was of relatively small magnitude and increased with speed and wave period. The force observed here was doubltess a result of carriage vibration.

On the heading $\chi = 45^0$, the sway force increased with increasing speed up to $Fr = .05$ to $.08$ and decreased at $Fr = .08$ to $.10$. The sway force then increased again at the high speeds $Fr = .25$. There was a consistent increase in force as the wave length increased from $\lambda/L = 0.5$ to $\lambda/L = 1.9$. There was also a consistent increase in force as the wave height increased from $h/\lambda = 1/40$ to $1/20$.

On the heading $\chi = 135^0$, the sway force exhibited similar tendencies as on the $\chi = 45^0$ heading except that the magnitude of the force was about 10 percent to 15 percent smaller. This reduced force was probably due to the greater amount of overhang at the stern and the associated curved hull surfaces. Any force acting normally to the hull surface on the after-body would have smaller horizontal component. Having smaller horizontal components, one would expect to find a smaller sway force.

In the case of the beam seas, $\chi = 90^0$, the sway force was of high magnitude. In all but two sets of experiments at $\lambda/L = 0.5$, the force could not be measured because the dynamometer was against the safety stops. The force acting on the model was greater than 30 pounds.

Yawing Moment

The amplitude of the oscillatory yawing moment is shown on Figs. 25 to 29 inclusive. As in the case of the sway force, there should be no yawing moment on the $\chi = 0^0$ and $\chi = 180^0$ headings. The yawing moment was of relatively small magnitude. There was a slight increase for a particular wave length with increasing speed. The greatest variation was found in the longer and steeper waves. This would indicate that the oscillatory yawing moment was associated with the velocity field established as the wave passes the model.

The maximum range in yawing moment was found on the $\chi = 45^0$ and the $\chi = 135^0$ headings. On the 135^0 heading there was about 25 percent increase in range of the oscillatory yawing moment as the speed increased from $Fr = 0$ to $Fr = 0.25$. This was in contrast to the other oblique heading $\chi = 45^0$ where there was little change in the oscillatory yawing moment with increasing speed.

In beam seas, $\chi = 90^0$, the maximum values of the oscillatory yawing moment occurred at the very low and high speeds. The minimum values were found at the intermediate speeds, $Fr = .08$ to $.12$.

In all cases the highest values of the oscillatory yawing moment was found in the steepest and longest waves. Very small values were experienced for the shortest waves $\lambda / L = 0.50$.

Drag Force

The amplitude of the oscillatory drag force is shown on Figs. 30 to 34 inclusive. The smallest range in oscillatory drag force was found in the beam seas, ($\chi = 90^0$). On this heading the change in drag was due to changes in the wetted surface of the hull because none of the flow field resulting from the passage of the wave had components parallel to the direction of travel.

The following sea and following quarter sea headings ($\chi = 0^0$ and 45^0) experienced about 25 percent larger range in oscillatory drag force than their corresponding head sea headings ($\chi = 135^0$ and 180^0). The largest range in oscillatory drag force occurred on the $\chi = 45^0$ heading. This behavior indicates that the greatest oscillatory drag force was associated with the smallest difference between the wave celerity and the component of the model speed parallel to the celerity vector. This line of reasoning then would indicate that the oscillatory drag should be smaller on the $\chi = 180^0$ than on the $\chi = 135^0$ which is found to be true by comparing Figs. 33 and 34.

The largest amplitude of oscillatory drag force was observed in the longest and steepest wave system on all headings. There was a general tendency for a 10 to 15 percent increase in range of force as the speed increased from 0 to $Fr = 0.25$.

Influence of Heading

Polar graphs have been prepared to give a clear picture of the influence of the angle of heading on the forces and moments acting on the model resulting from the wave forces. These graphs are Figs. 35 to 40 inclusive. The data used in constructing these figures were obtained from the maximum values from the previous series of graphs (Figs. 5 to 35 inclusive).

Separate lines were drawn for each wave length.

Figure 35 shows the data for the oscillatory heave force. The longer wave lengths exhibit a maximum range of force on the $\chi = 45^0$ heading. The shortest wave length, $\lambda/L = 0.5$, experienced maximum heave force in the beam seas, $\chi = 90^0$.

The pitching moment comparison is shown on Fig. 36. The greatest range in oscillatory pitching moment was found on the $\chi = 0^0$ and $\chi = 45^0$ headings. The minimum values of pitching were found on the $\chi = 90^0$. The shortest wave length $\lambda/L = 0.50$ exhibited a negligible range in pitching moment on any heading as was expected. The pitching moment experienced on the $\chi = 90^0$ heading results from the longitudinal asymmetry of the fullness of the hull sections. Even though the longitudinal axis of the hull was parallel to the wave crests, the fore-body experiences the increased draught of the oncoming wave before the after-body. The sections of fore-body are much fuller (see Fig. 1, page 43, reference 1), than the corresponding sections of the after-body, thus the increased buoyancy resulting from the wave was experienced first by the fore-body resulting in a pitching moment on the restrained model. This would not happen if the hull had perfectly symmetrical sections fore and aft.

The range in oscillatory sway force is shown on Fig. 37. The range in sway force was negligible on the $\chi = 0^0$ and $\chi = 180^0$ headings. The sway force increased to very large values in the beam seas ($\chi = 90^0$). The range of force was beyond the measuring capacity of the six-component balance for all but the shortest waves ($\lambda/L = 0.5$) on the $\chi = 90^0$ heading.

The influence of the angle of heading on the range of yawing moment is summarized on a polar graph, Fig. 38. The oscillatory yawing moment was negligible in head and following seas, $\chi = 0^0$ and $\chi = 180^0$. Large values were observed on the $\chi = 45^0$ and $\chi = 135^0$ headings. Smaller values of the range in yawing moment were found in beam seas ($\chi = 90^0$). The presence of a yawing moment here was due to the longitudinal asymmetry in the reflection coefficients of the waves from the side of the hull. The fore-body is nearly wall-sided throughout its length. On the other hand, the after-body and particularly the stern is characterized by large overhang.

The variation of the range of rolling moment and heading angle was summarized on Fig. 39. As was expected, the greatest range in rolling moment was observed in the beam seas ($\chi = 90^0$). Large range of rolling moment was observed in head seas ($\chi = 180^0$). The greatest difference between model speed and wave celerity exists on this heading. This rolling moment was probably due to the asymmetrical shedding of vortices in the wake of the ship.

The comparison of the range in drag force with heading angle is shown on Fig. 40. This graph indicates that the greatest range of drag force was observed on the $\chi = 45^0$ heading. The next largest range was found on the $\chi = 135^0$ heading. The largest range in drag force was associated with those waves which were approximately equal to length of the hull, $\lambda/L = 0.9$. When the waves were longer or shorter than this, the range of drag force was smaller.

V. CONCLUSIONS

These conclusions may be developed from the tests on the restrained model in waves. The force and moment histories as measured with a strain-gauge type six-component balance were separated into two parts; the steady-state and the oscillatory forces and moments. The oscillatory forces and moments are those which are the result of the passage of the waves. The oscillatory forces and moments are shown as a range in force or double amplitude.

1. The oscillatory heave force was slightly speed dependent in the longer waves. The largest values were found in the longest waves and steepest waves.

2. The oscillatory pitching moment increased with increasing speed in nearly all cases. Two exceptions occurred on the longer waves and on the $\chi = 0^0$ heading. The oscillatory pitching moment always increased with increasing wave steepness.

3. The oscillatory rolling moment decreased generally as the Froude number increased from 0 to .05. Minimum values were observed between $.05 < Fr < .1$. The range of the rolling moment then increases with a further increase in speed. The oscillatory rolling moment was more dependent upon wave steepness than on wave length.

4. The oscillatory sway force exhibited a complex relationship between Froude number 0 and 0.1. The range of sway force increased consistently with increasing speed at $Fr > 0.1$. The sway force increased with increasing wave length and wave steepness.

5. The oscillatory yawing moment was slightly speed dependent, increasing with increasing speed. The yawing moment increased with increasing wave length and wave steepness.

6. The oscillatory drag force increased about 10 percent to 15 percent as the speed increased from Fr = 0 to .25. The range in drag force was always smaller in the shortest wave length, but there was little relationship between wave length and wave steepness in the longer waves.

The effect of the angle of heading on the forces and moments acting on the restrained model are summarized separately.

1. The maximum range of oscillatory heave force was experienced on $\chi = 45^0$ heading for all but the shortest waves. The shortest waves ($\lambda/L = 0.5$) experienced the maximum heave force in the beam seas. (See Fig. 35.)

2. The maximum range of oscillatory pitching moment was observed on the $\chi = 0^0$ and $\chi = 45^0$ headings. The minimum pitching moment was found on the $\chi = 90^0$ heading. The range of pitching moment showed little variation with angle of heading for the shortest wave length $\lambda/L = 0.5$. (See Fig. 36).

3. Very large values of range of oscillatory sway force were experienced on the $\chi = 90^0$ heading. In some instances measurements could not be obtained because the force exceeded the capacity of the force balance. (See Fig. 37.)

4. The maximum range in yawing moment was observed on the two oblique headings, $\chi = 45^0$ and $\chi = 135^0$. Smallest range in yawing moment was found on the $\chi = 90^0$ heading. (See Fig. 38.)

5. The maximum range in oscillatory rolling moment was observed in the beam seas ($\chi = 90^0$ heading). Minimum oscillatory rolling moment was observed on the $\chi = 0^0$ heading.

6. The maximum range in oscillatory drag force was found on the $\chi = 45^0$ and $\chi = 135^0$ headings.

REFERENCES

1. Schulz, E. F., Restrained model tests in head seas. Fort Collins, Colorado State University, Civil Engineering Department. CER59EFS7, March 1959.

2. Schulz, E. F., T. T. Williams, and R. M. Ralston. Model tests with a tanker in oblique seas. Fort Collins, Colorado State University, Civil Engineering Department, CER57EFS2, January 1957.

3. Couch, E. B., and M. St. Denis, Comparison of power performances of ten 600-foot single-screw tanker hulls as predicted from model tests. Trans. SNAME New York, V. 56 pp. 359-394, 416-421, November 1948.

TABLE 1

Model Particulars

L_{WL}	Length on waterline, ft	5
B	Maximum beam at waterline, ft	0.69
H	Draft at even keel, ft	0.27
Δ	Displacement of hull, lbs	46.2
Scale factor of ship to model length		120
$1/2\ \alpha$	Entrance angle on waterline	27.5°
C_B	Block coefficient	0.746
C_M	Maximum (midship) section coefficient	0.993
C_P	Prismatic coefficient	0.752
C_W	Waterplane coefficient	0.821

TABLE 2

Wave Length and Height

Wave Length λ (feet)	Relative Wave Length λ/L	Wave Steepness h/λ
2.4	0.48	1/40
		1/30
		1/20
5.6	0.9	1/40
		1/30
		1/20
7.2	1.45	1/40
		1/30
9.4	1.9	1/40

TABLE 3

Model Headings

Heading Angle χ	Description
0	Following seas
45	Waves approaching from after quarter
90	Waves approaching from the beam
135	Waves approaching from forward quarter
180	Head seas

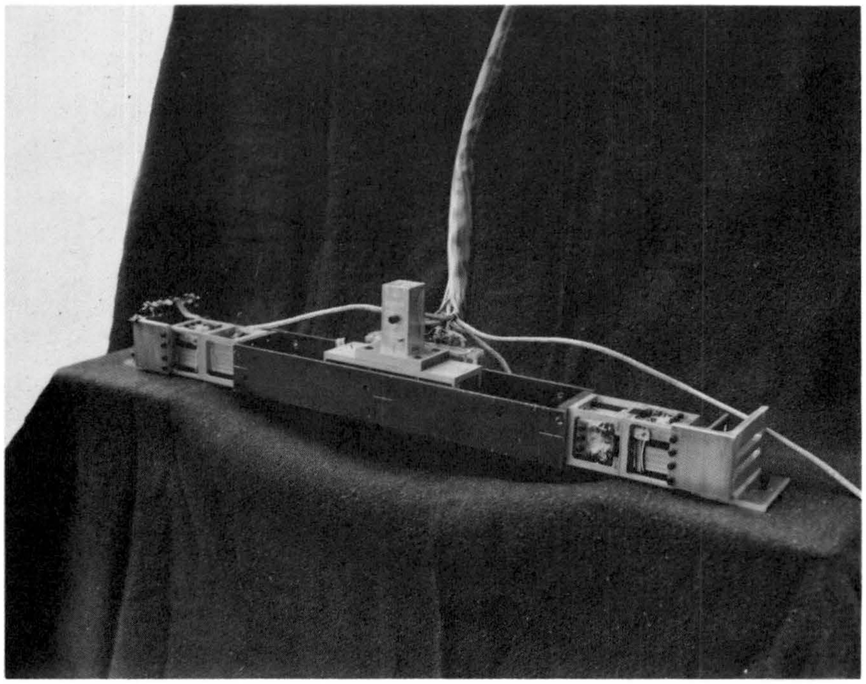

Figure 1. Six-Component Balance

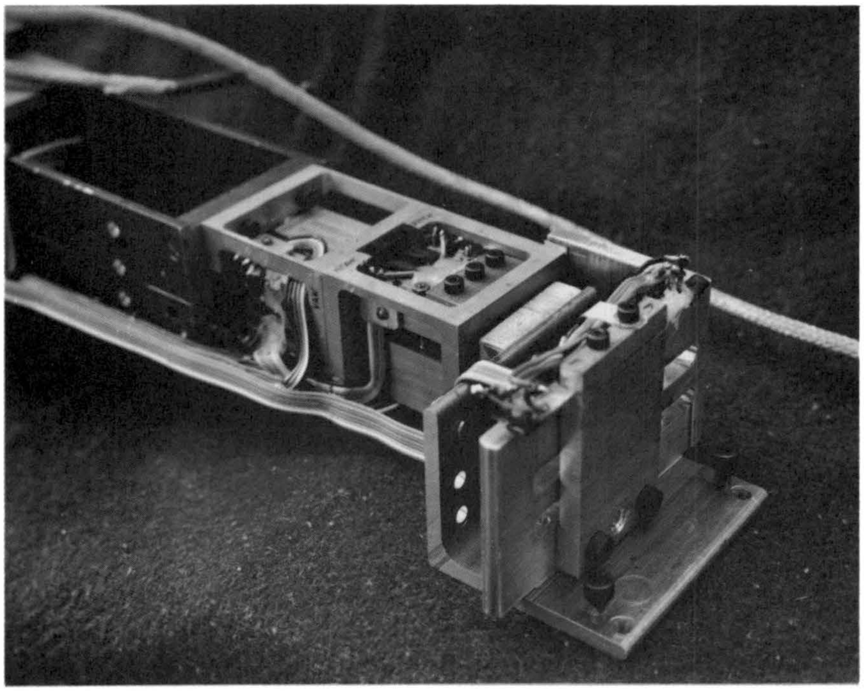

Figure 2. Forward Force Unit
Six-Component Balance

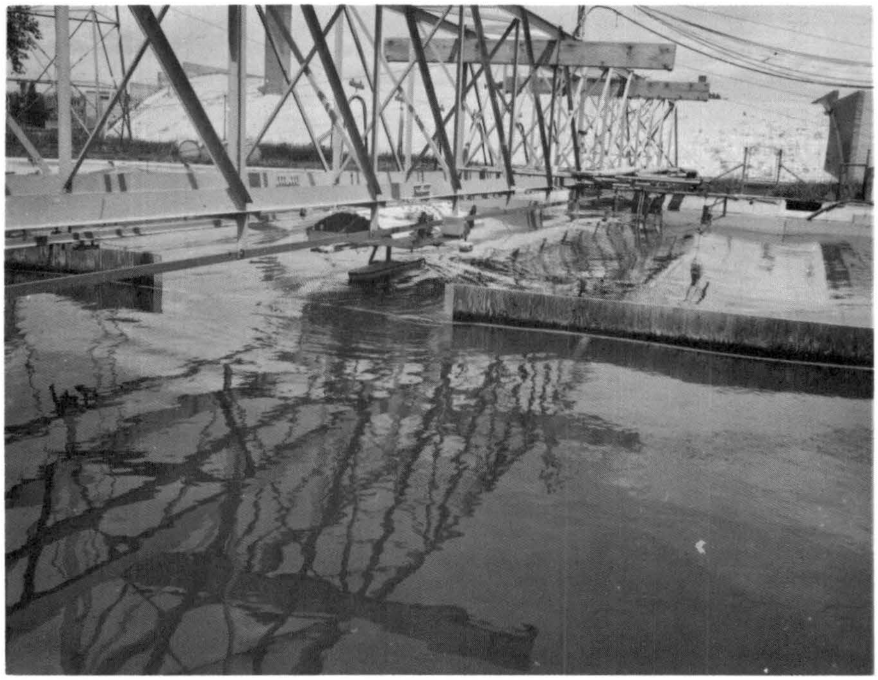

Figure 3. Towing Bridge and Wave Basin Test in Beam Seas, $\chi = 90^0$

Figure 4. Model Tanker - Test at $\chi = 90^0$

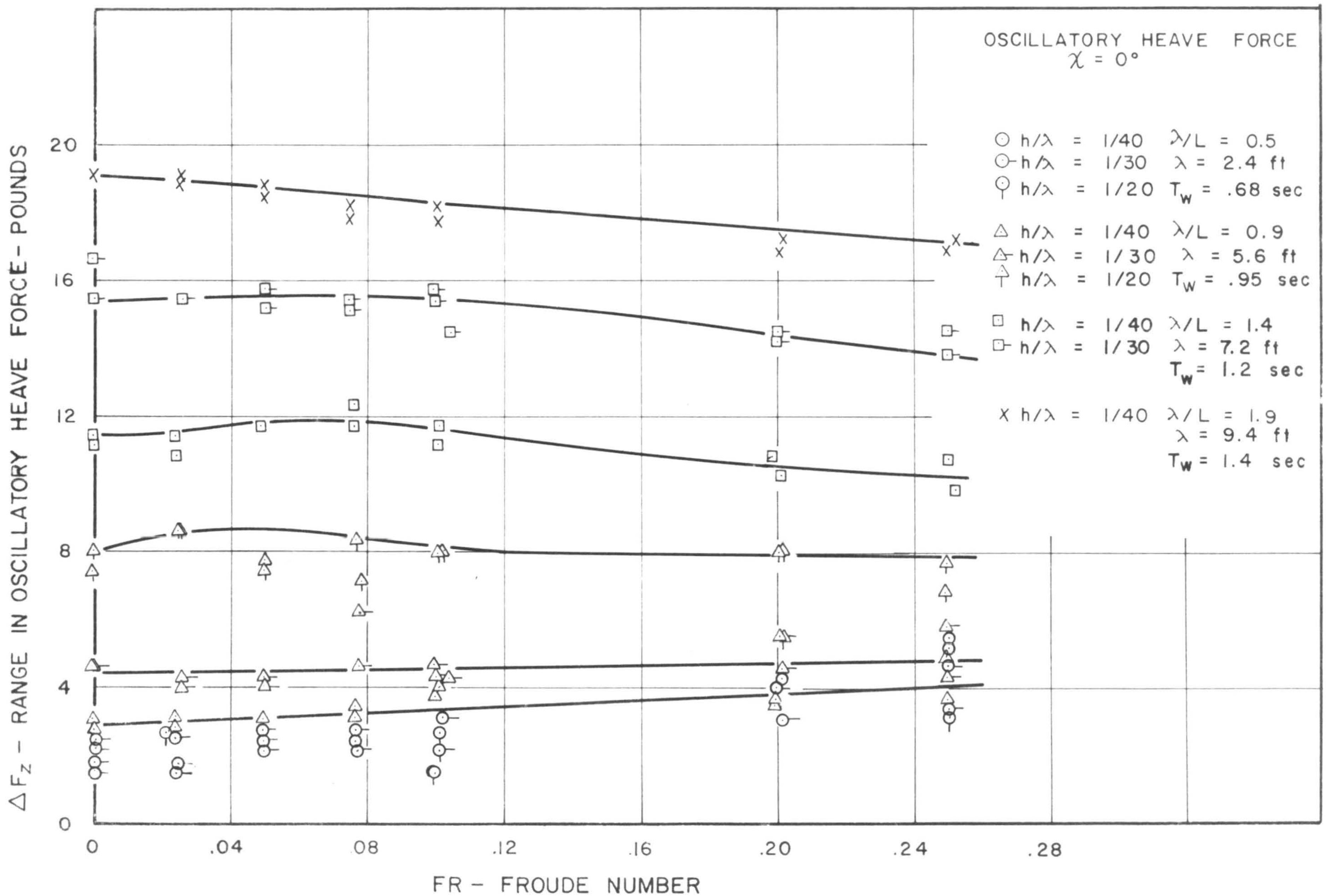

OSCILLATORY HEAVE FORCE
χ = 0°
h/λ = 1/40 λ/L = 0.5
h/λ = 1/30 λ = 2.4 ft
h/λ = 1/20 T_W = .68 sec
h/λ = 1/40 λ/L = 0.9
h/λ = 1/30 λ = 5.6 ft
h/λ = 1/20 T_W = .95 sec
h/λ = 1/40 λ/L = 1.4
h/λ = 1/30 λ = 7.2 ft
T_W = 1.2 sec
X h/λ = 1/40 λ/L = 1.9
λ = 9.4 ft
T_W = 1.4 sec
ΔF_Z - RANGE IN OSCILLATORY HEAVE FORCE - POUNDS
0
4
8
12
16
20
0
.04
.08
.12
.16
.20
.24
.28
FR - FROUDE NUMBER

FIG. 5

FIG. 5

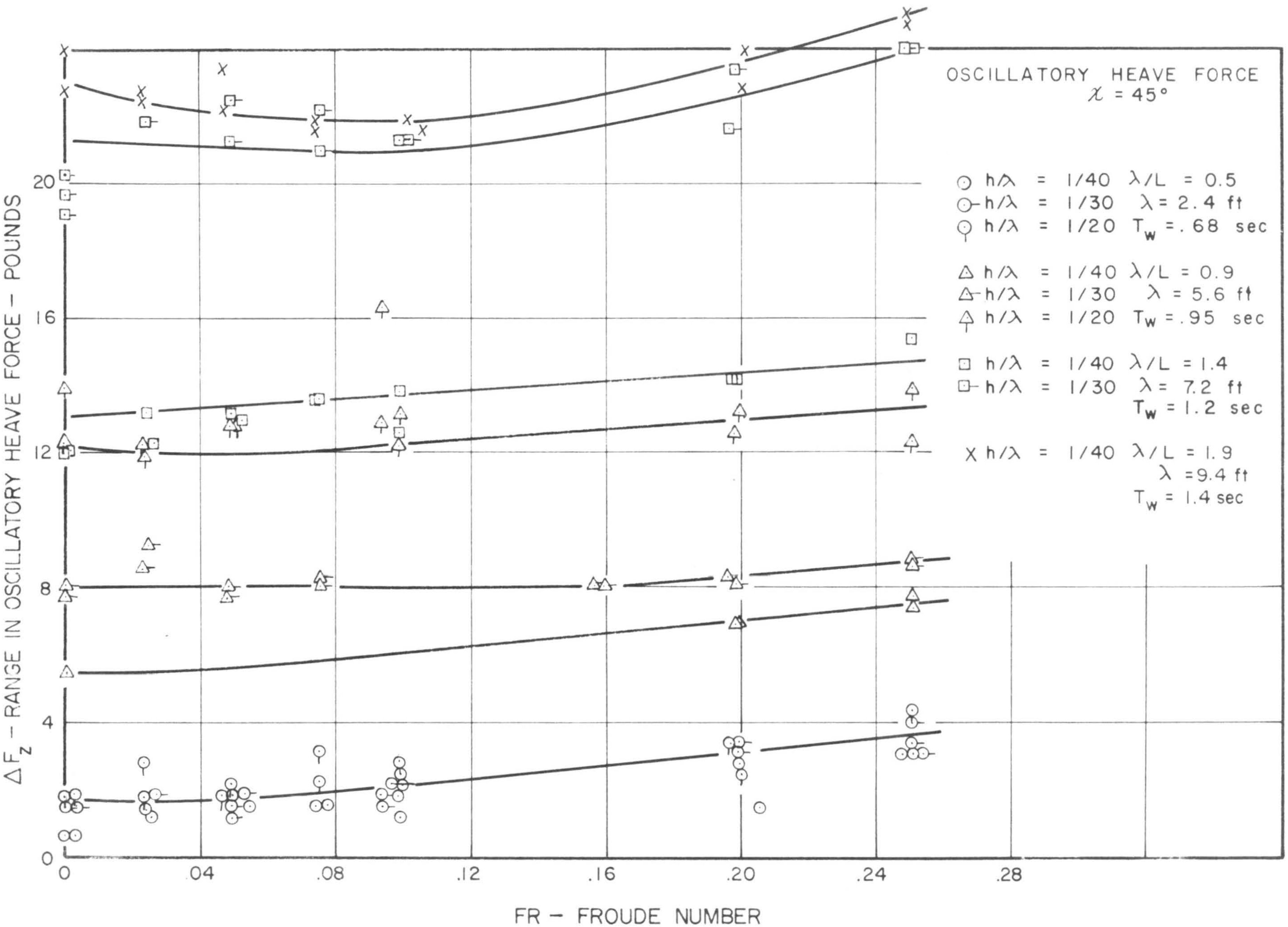

OSCILLATORY HEAVE FORCE
χ = 45°
h/λ = 1/40 λ/L = 0.5
h/λ = 1/30 λ = 2.4 ft
h/λ = 1/20 T_w = .68 sec
h/λ = 1/40 λ/L = 0.9
h/λ = 1/30 λ = 5.6 ft
h/λ = 1/20 T_w = .95 sec
h/λ = 1/40 λ/L = 1.4
h/λ = 1/30 λ = 7.2 ft
T_w = 1.2 sec
X h/λ = 1/40 λ/L = 1.9
λ = 9.4 ft
T_w = 1.4 sec
ΔF_z - RANGE IN OSCILLATORY HEAVE FORCE - POUNDS
FR - FROUDE NUMBER
0
4
8
12
16
20
.04
.08
.12
.16
.20
.24
.28

FIG. 6

FIG. 6

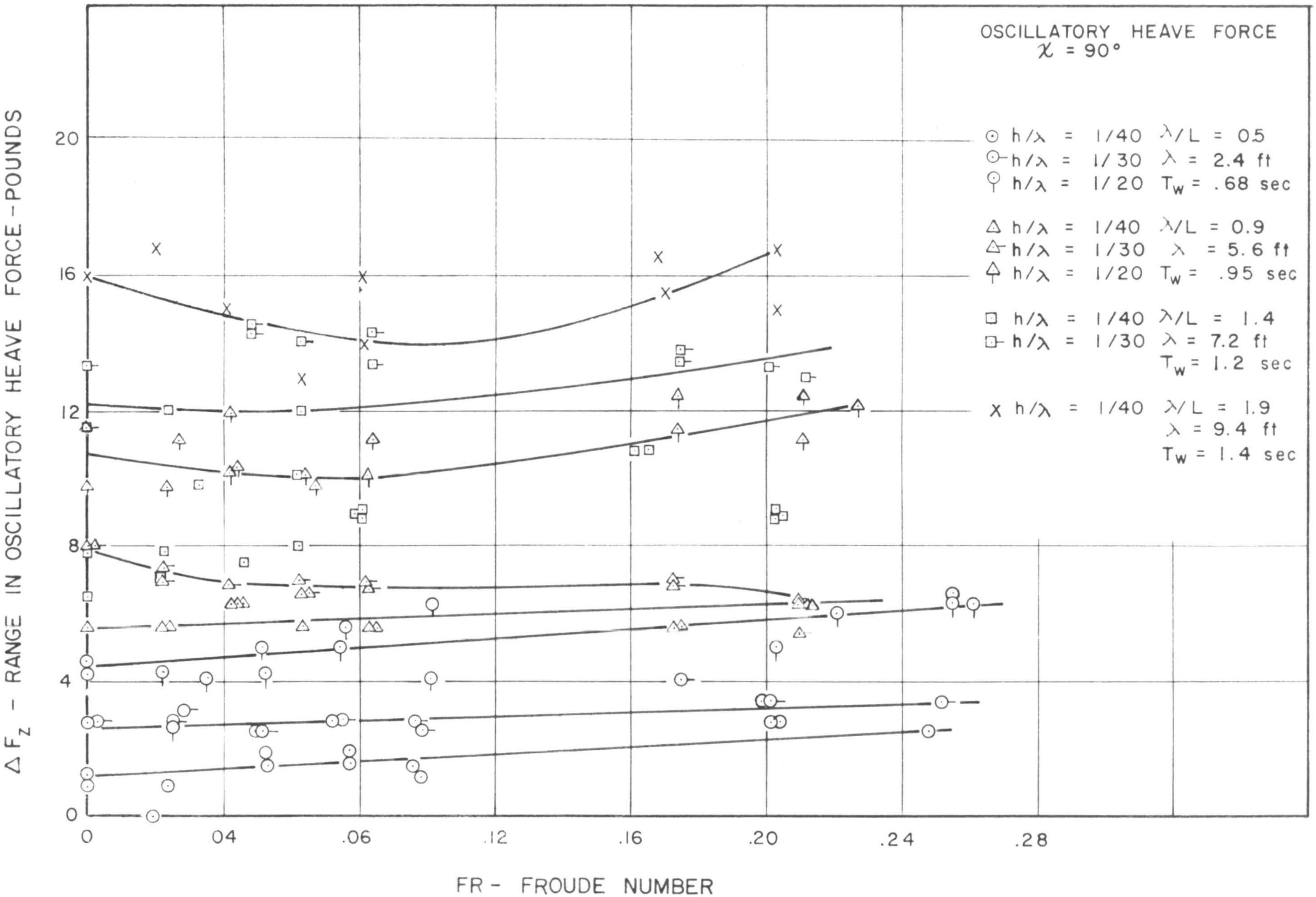
OSCILLATORY HEAVE FORCE
χ = 90°
⊙ h/λ = 1/40 λ/L = 0.5
⊙- h/λ = 1/30 λ = 2.4 ft
h/λ = 1/20 T_W = .68 sec
△ h/λ = 1/40 λ/L = 0.9
△- h/λ = 1/30 λ = 5.6 ft
h/λ = 1/20 T_W = .95 sec
□ h/λ = 1/40 λ/L = 1.4
□- h/λ = 1/30 λ = 7.2 ft
T_W = 1.2 sec
X h/λ = 1/40 λ/L = 1.9
λ = 9.4 ft
T_W = 1.4 sec
Δ F_Z - RANGE IN OSCILLATORY HEAVE FORCE - POUNDS
FR - FROUDE NUMBER
0
4
8
12
16
20
0
.04
.06
.12
.16
.20
.24
.28
FIG. 7

FIG. 7

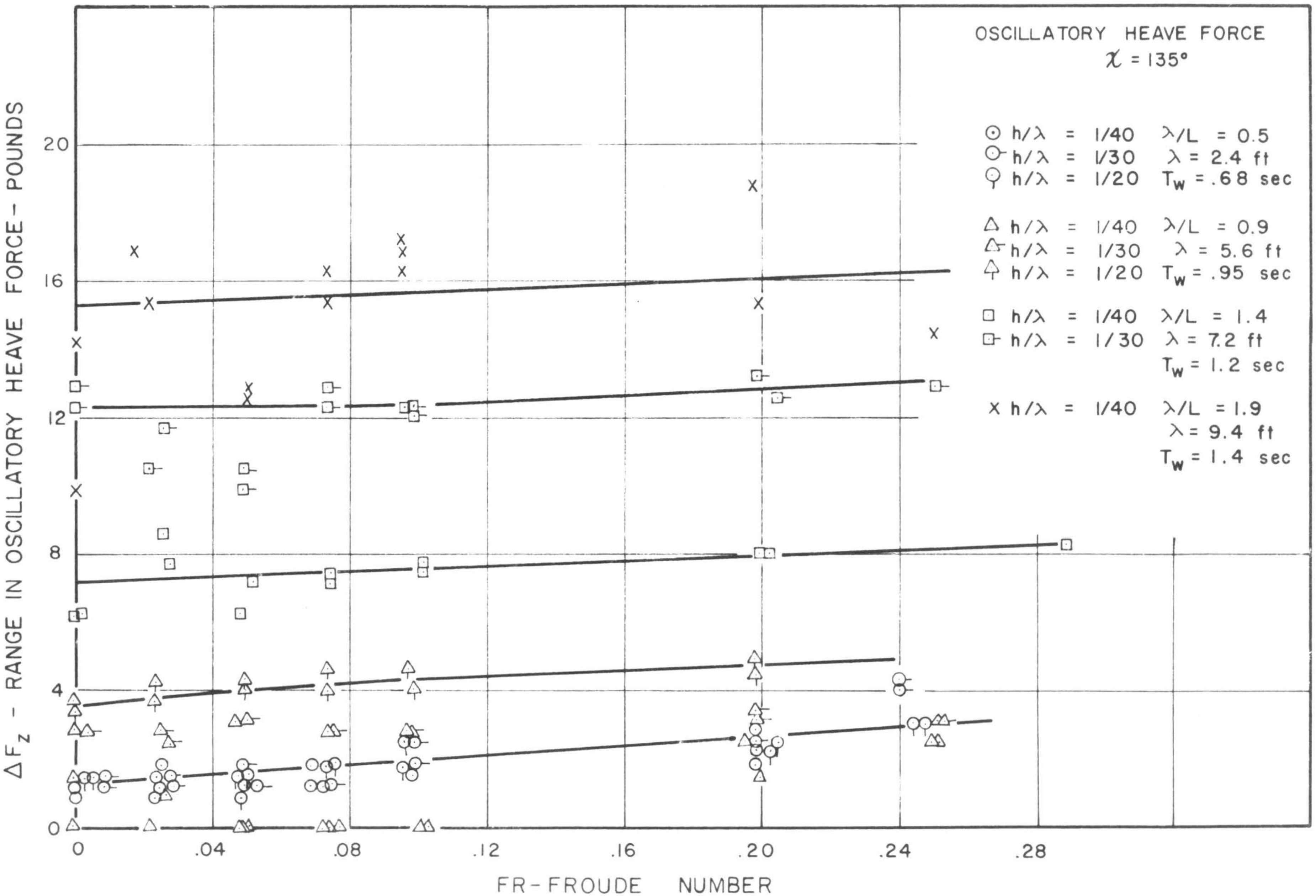
OSCILLATORY HEAVE FORCE
χ = 135°
h/λ = 1/40 λ/L = 0.5
h/λ = 1/30 λ = 2.4 ft
h/λ = 1/20 Tw = .68 sec
h/λ = 1/40 λ/L = 0.9
h/λ = 1/30 λ = 5.6 ft
h/λ = 1/20 Tw = .95 sec
h/λ = 1/40 λ/L = 1.4
h/λ = 1/30 λ = 7.2 ft
Tw = 1.2 sec
X h/λ = 1/40 λ/L = 1.9
λ = 9.4 ft
Tw = 1.4 sec
ΔFz - RANGE IN OSCILLATORY HEAVE FORCE - POUNDS
FR - FROUDE NUMBER
0
4
8
12
16
20
0
.04
.08
.12
.16
.20
.24
.28

FIG. 8

FIG. 8

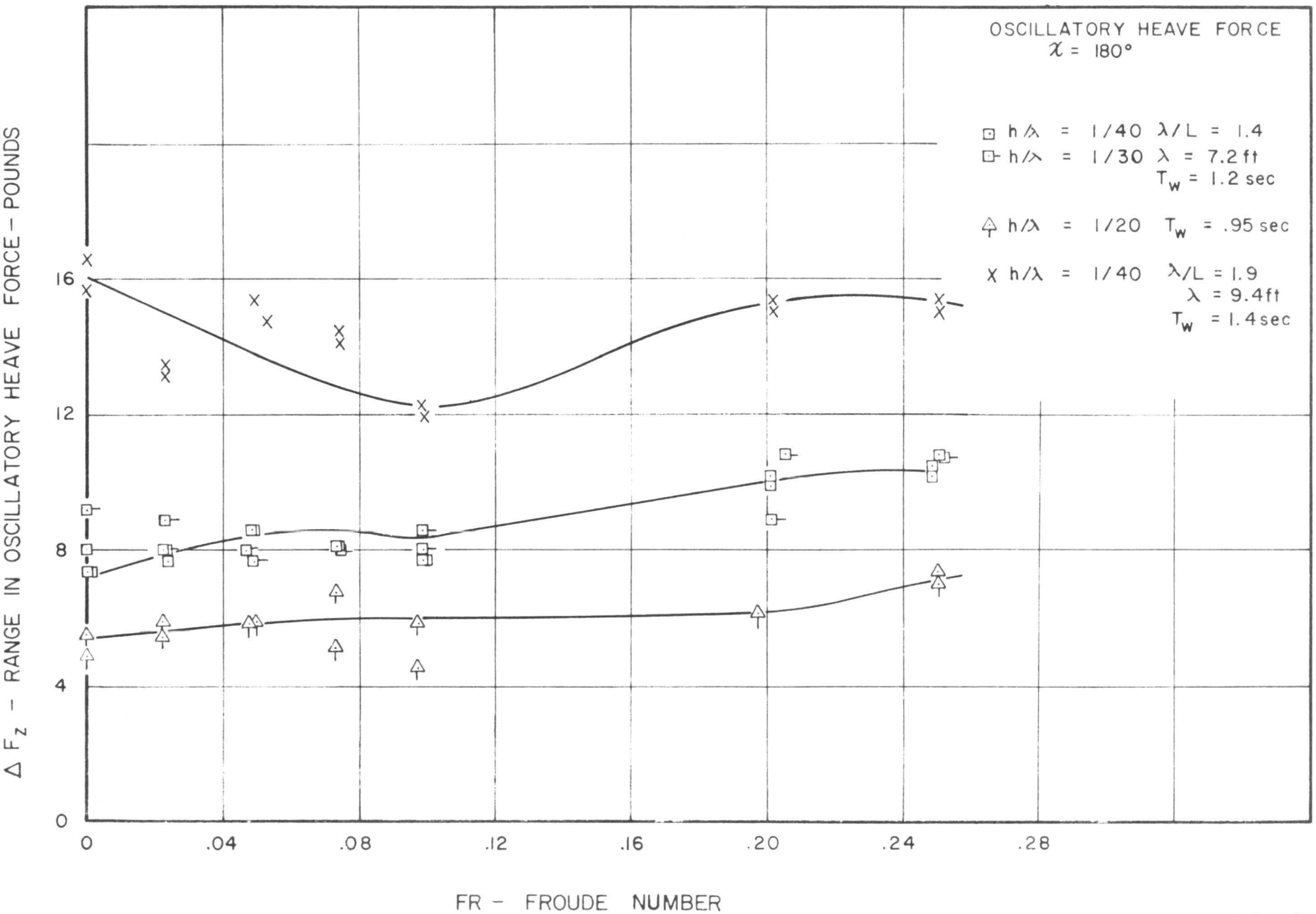
OSCILLATORY HEAVE FORCE
χ = 180°
h/λ = 1/40 λ/L = 1.4
h/λ = 1/30 λ = 7.2 ft
T_W = 1.2 sec
h/λ = 1/20 T_W = .95 sec
h/λ = 1/40 λ/L = 1.9
λ = 9.4ft
T_W = 1.4 sec
ΔF_Z - RANGE IN OSCILLATORY HEAVE FORCE - POUNDS
0
4
8
12
16
0
.04
.08
.12
.16
.20
.24
.28
FR - FROUDE NUMBER

FIG. 9

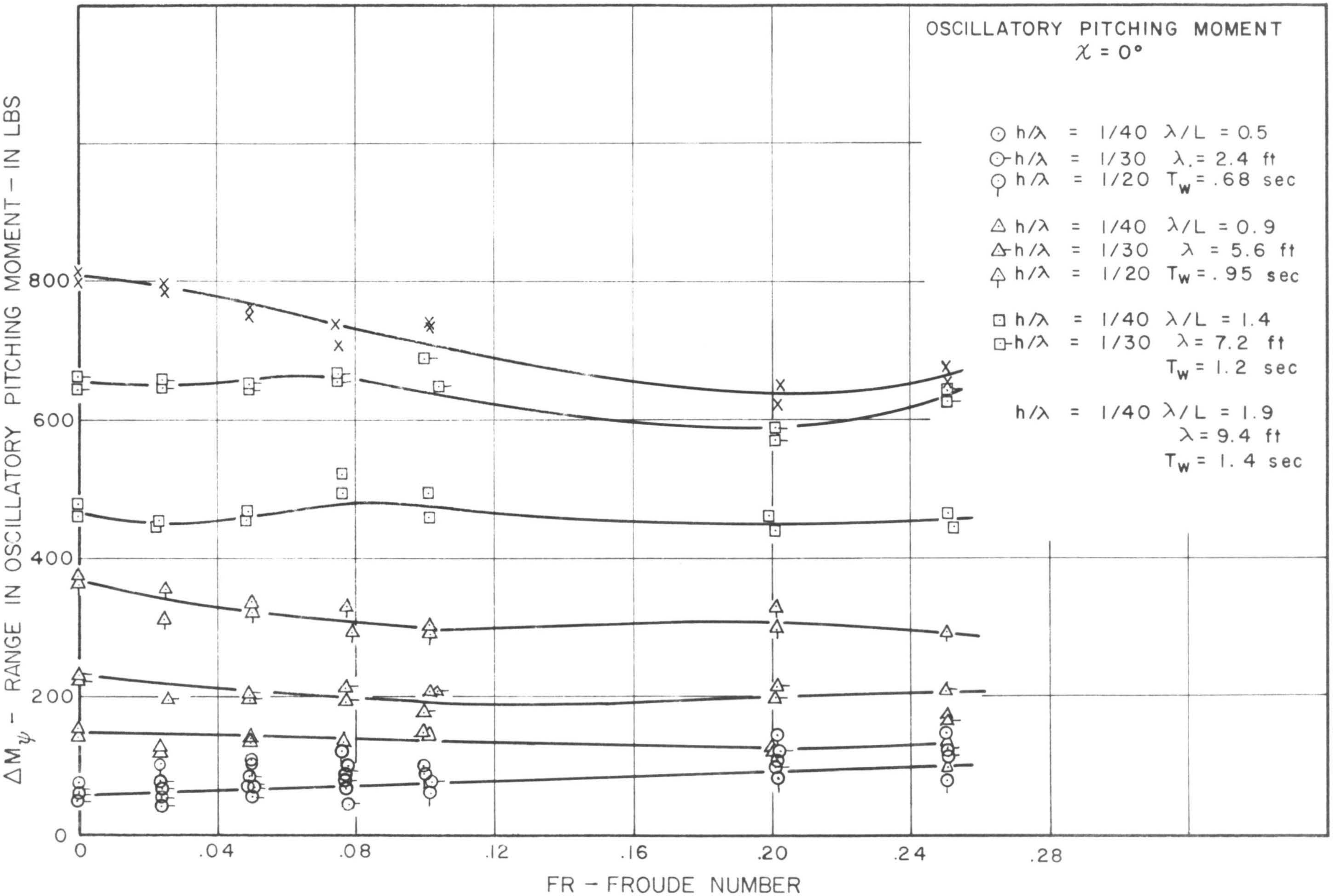

OSCILLATORY PITCHING MOMENT
χ = 0°
h/λ = 1/40 λ/L = 0.5
h/λ = 1/30 λ = 2.4 ft
h/λ = 1/20 Tw = .68 sec
h/λ = 1/40 λ/L = 0.9
h/λ = 1/30 λ = 5.6 ft
h/λ = 1/20 Tw = .95 sec
h/λ = 1/40 λ/L = 1.4
h/λ = 1/30 λ = 7.2 ft
Tw = 1.2 sec
h/λ = 1/40 λ/L = 1.9
λ = 9.4 ft
Tw = 1.4 sec
ΔMψ - RANGE IN OSCILLATORY PITCHING MOMENT - IN LBS
800
600
400
200
0
0
.04
.08
.12
.16
.20
.24
.28
FR - FROUDE NUMBER

FIG. 10

FIG. 10

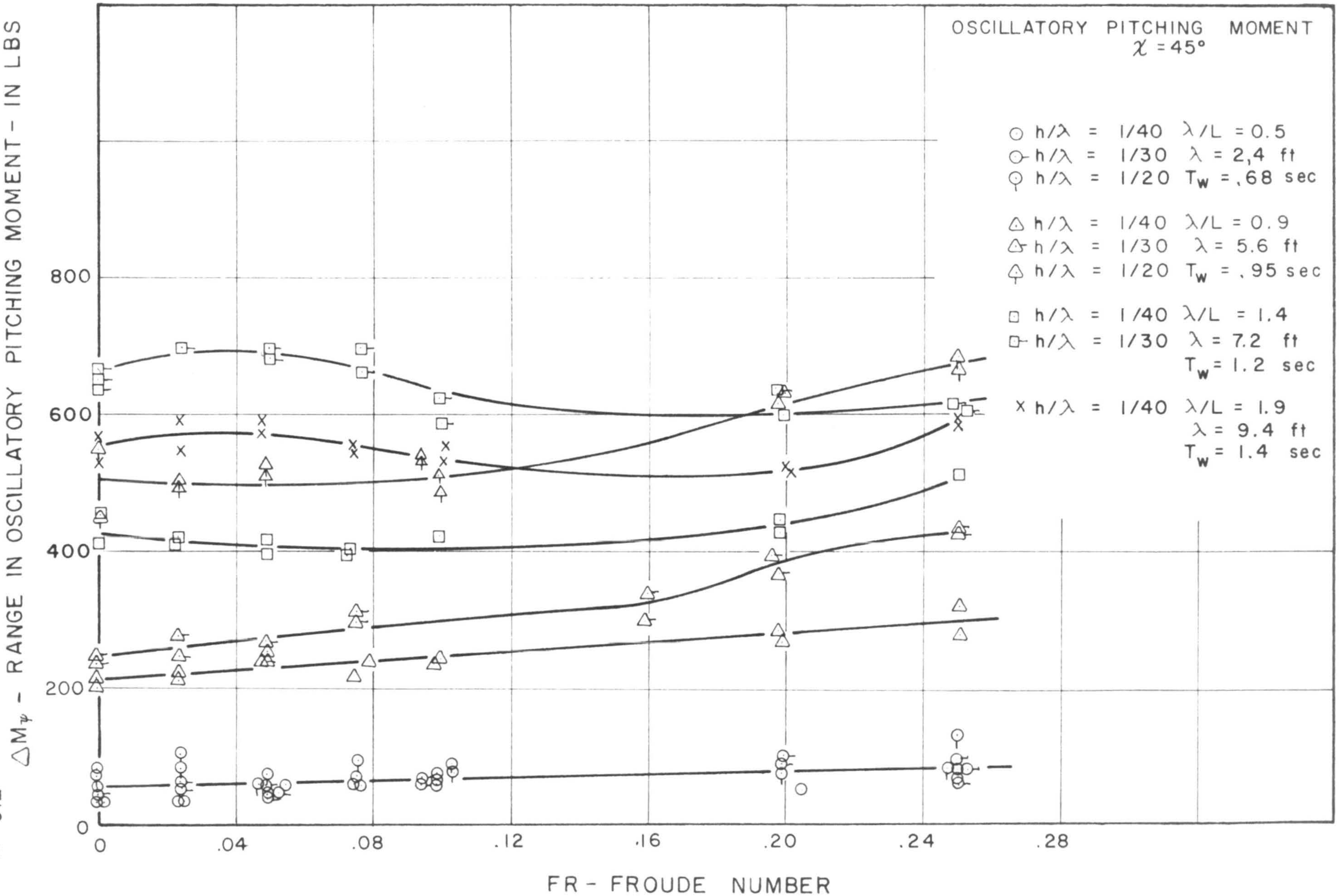

OSCILLATORY PITCHING MOMENT
$\chi = 45°$
○ h/λ = 1/40 λ/L = 0.5
○- h/λ = 1/30 λ = 2,4 ft
○ h/λ = 1/20 T_W = ,68 sec
△ h/λ = 1/40 λ/L = 0.9
△- h/λ = 1/30 λ = 5.6 ft
△ h/λ = 1/20 T_W = ,95 sec
□ h/λ = 1/40 λ/L = 1.4
□- h/λ = 1/30 λ = 7.2 ft
T_W = 1.2 sec
× h/λ = 1/40 λ/L = 1.9
λ = 9.4 ft
T_W = 1.4 sec
ΔM_ψ - RANGE IN OSCILLATORY PITCHING MOMENT - IN LBS
800
600
400
200
0
0
.04
.08
.12
.16
.20
.24
.28
FR - FROUDE NUMBER

FIG. 11

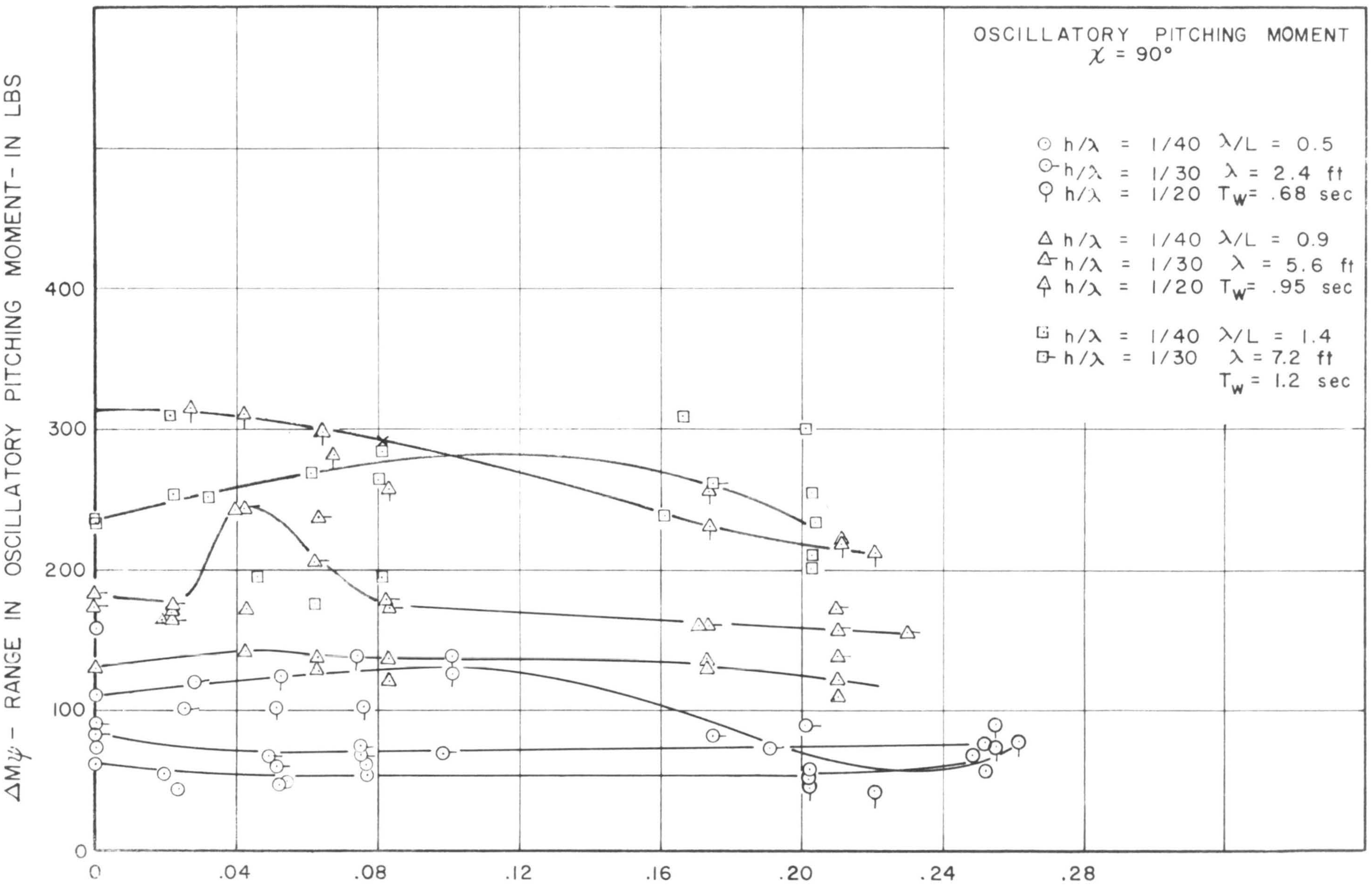

OSCILLATORY PITCHING MOMENT
χ = 90°
h/λ = 1/40 λ/L = 0.5
h/λ = 1/30 λ = 2.4 ft
h/λ = 1/20 T_W = .68 sec
h/λ = 1/40 λ/L = 0.9
h/λ = 1/30 λ = 5.6 ft
h/λ = 1/20 T_W = .95 sec
h/λ = 1/40 λ/L = 1.4
h/λ = 1/30 λ = 7.2 ft
T_W = 1.2 sec
ΔM_ψ - RANGE IN OSCILLATORY PITCHING MOMENT - IN LBS
0
100
200
300
400
0
.04
.08
.12
.16
.20
.24
.28
FR - FROUDE NUMBER

FIG. 12

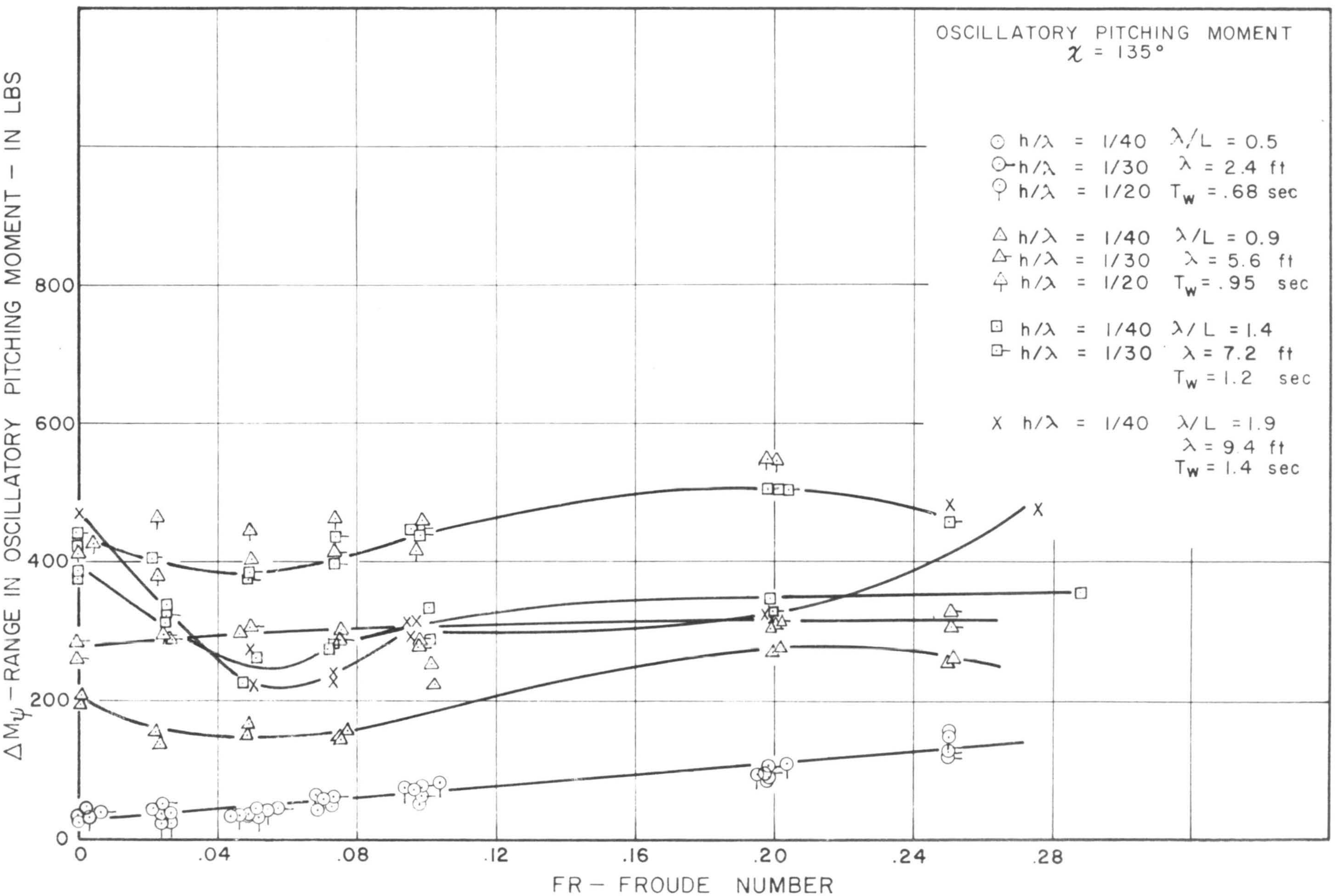
OSCILLATORY PITCHING MOMENT
χ = 135°
h/λ = 1/40 λ/L = 0.5
h/λ = 1/30 λ = 2.4 ft
h/λ = 1/20 T_W = .68 sec
h/λ = 1/40 λ/L = 0.9
h/λ = 1/30 λ = 5.6 ft
h/λ = 1/20 T_W = .95 sec
h/λ = 1/40 λ/L = 1.4
h/λ = 1/30 λ = 7.2 ft
T_W = 1.2 sec
X h/λ = 1/40 λ/L = 1.9
λ = 9.4 ft
T_W = 1.4 sec
ΔM_ψ – RANGE IN OSCILLATORY PITCHING MOMENT – IN LBS
0
200
400
600
800
0
.04
.08
.12
.16
.20
.24
.28
FR – FROUDE NUMBER

FIG. 13

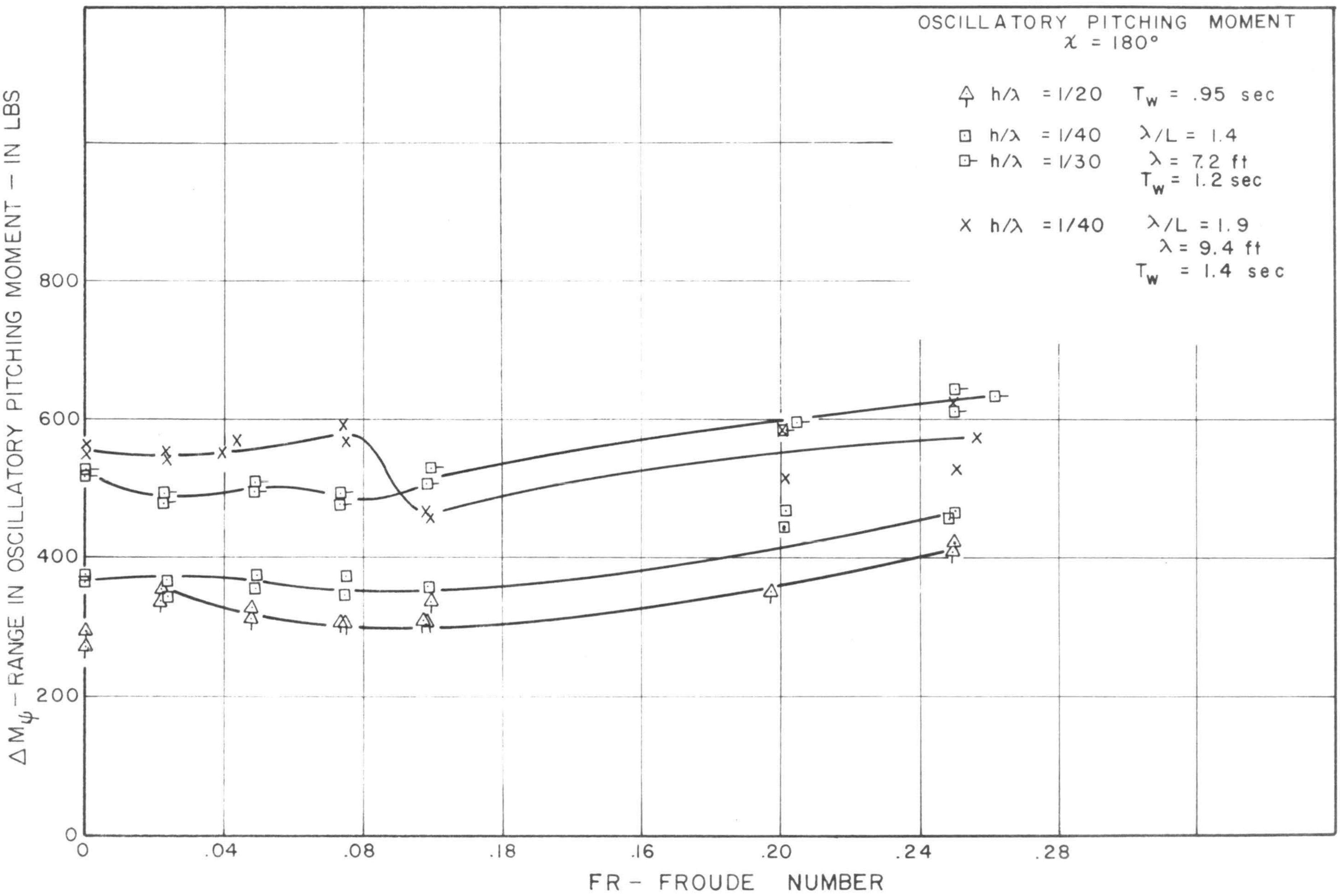
OSCILLATORY PITCHING MOMENT
χ = 180°
h/λ = 1/20 T_w = .95 sec
h/λ = 1/40 λ/L = 1.4
h/λ = 1/30 λ = 7.2 ft
T_w = 1.2 sec
X h/λ = 1/40 λ/L = 1.9
λ = 9.4 ft
T_w = 1.4 sec
ΔM_ψ – RANGE IN OSCILLATORY PITCHING MOMENT – IN LBS
0
200
400
600
800
0
.04
.08
.18
.16
.20
.24
.28
FR – FROUDE NUMBER

FIG. 14

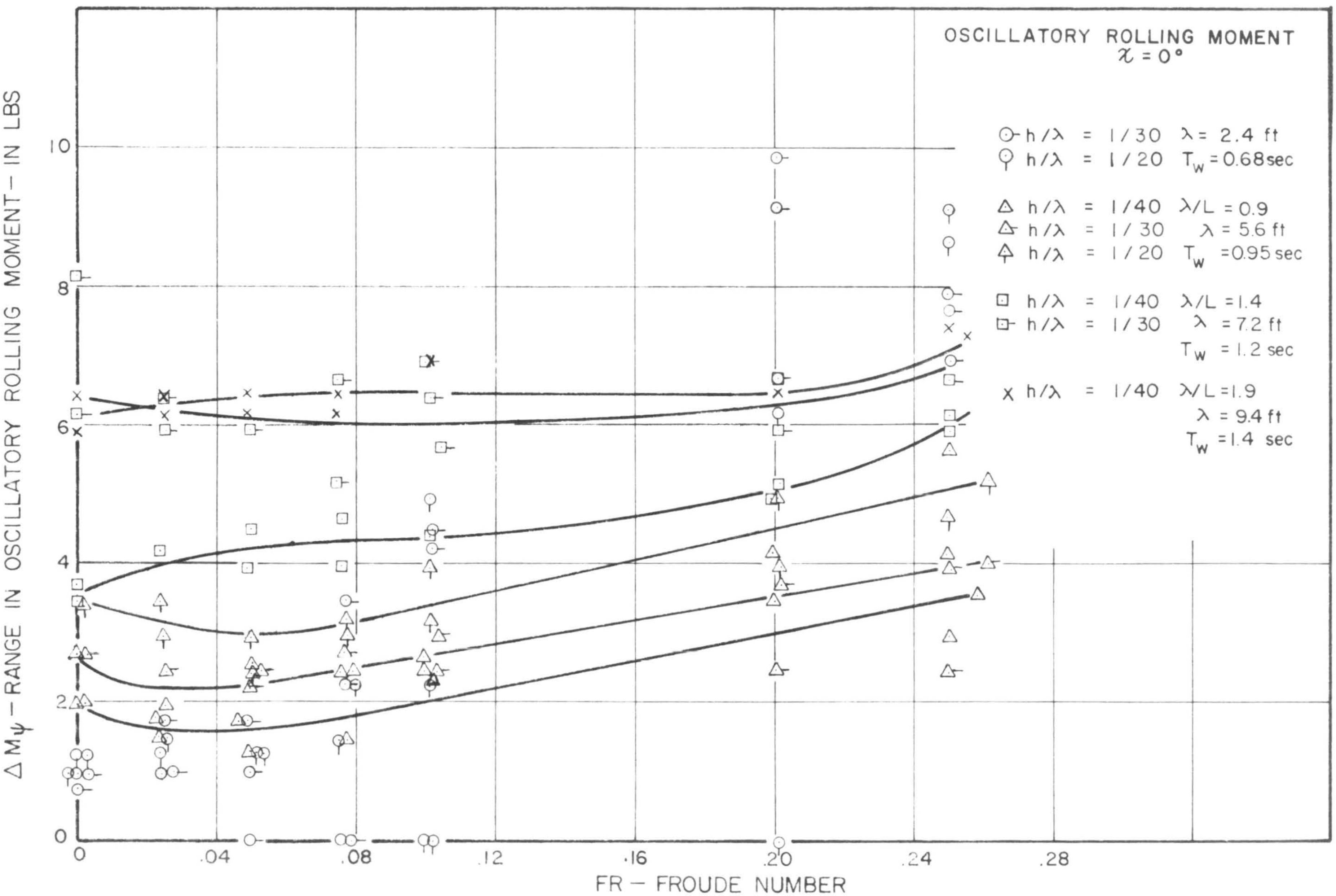

OSCILLATORY ROLLING MOMENT
χ = 0°
h/λ = 1/30 λ = 2.4 ft
h/λ = 1/20 T_W = 0.68 sec
h/λ = 1/40 λ/L = 0.9
h/λ = 1/30 λ = 5.6 ft
h/λ = 1/20 T_W = 0.95 sec
h/λ = 1/40 λ/L = 1.4
h/λ = 1/30 λ = 7.2 ft
T_W = 1.2 sec
h/λ = 1/40 λ/L = 1.9
λ = 9.4 ft
T_W = 1.4 sec
ΔMψ – RANGE IN OSCILLATORY ROLLING MOMENT – IN LBS
FR – FROUDE NUMBER
0
2
4
6
8
10
.04
.08
.12
.16
.20
.24
.28
FIG. 15

FIG. 15

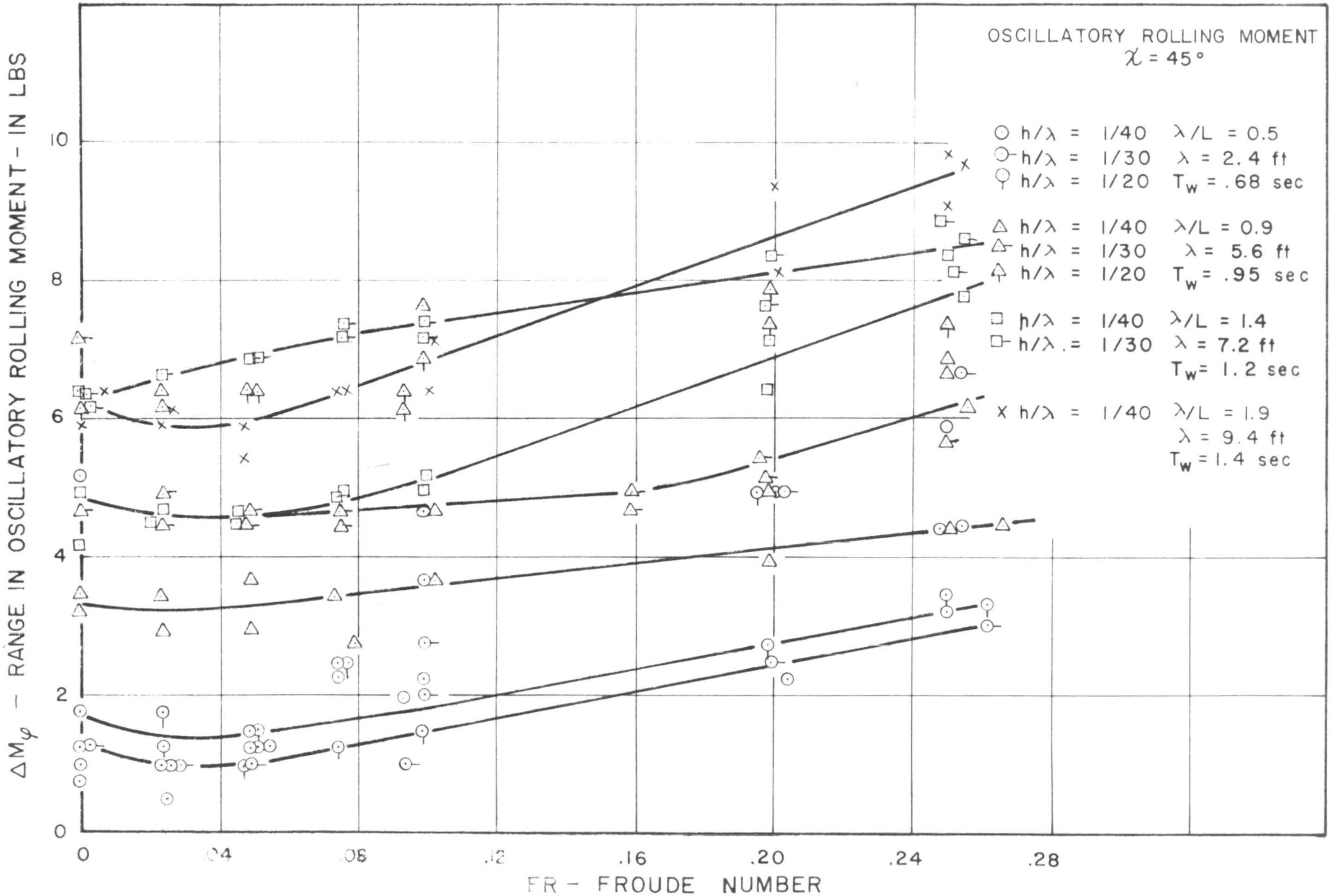

OSCILLATORY ROLLING MOMENT
χ = 45°
h/λ = 1/40 λ/L = 0.5
h/λ = 1/30 λ = 2.4 ft
h/λ = 1/20 T_w = .68 sec
h/λ = 1/40 λ/L = 0.9
h/λ = 1/30 λ = 5.6 ft
h/λ = 1/20 T_w = .95 sec
h/λ = 1/40 λ/L = 1.4
h/λ = 1/30 λ = 7.2 ft
T_w = 1.2 sec
X h/λ = 1/40 λ/L = 1.9
λ = 9.4 ft
T_w = 1.4 sec
ΔM_φ - RANGE IN OSCILLATORY ROLLING MOMENT - IN LBS
0
2
4
6
8
10
0
.04
.08
.12
.16
.20
.24
.28
FR - FROUDE NUMBER

FIG. 16

FIG. 16

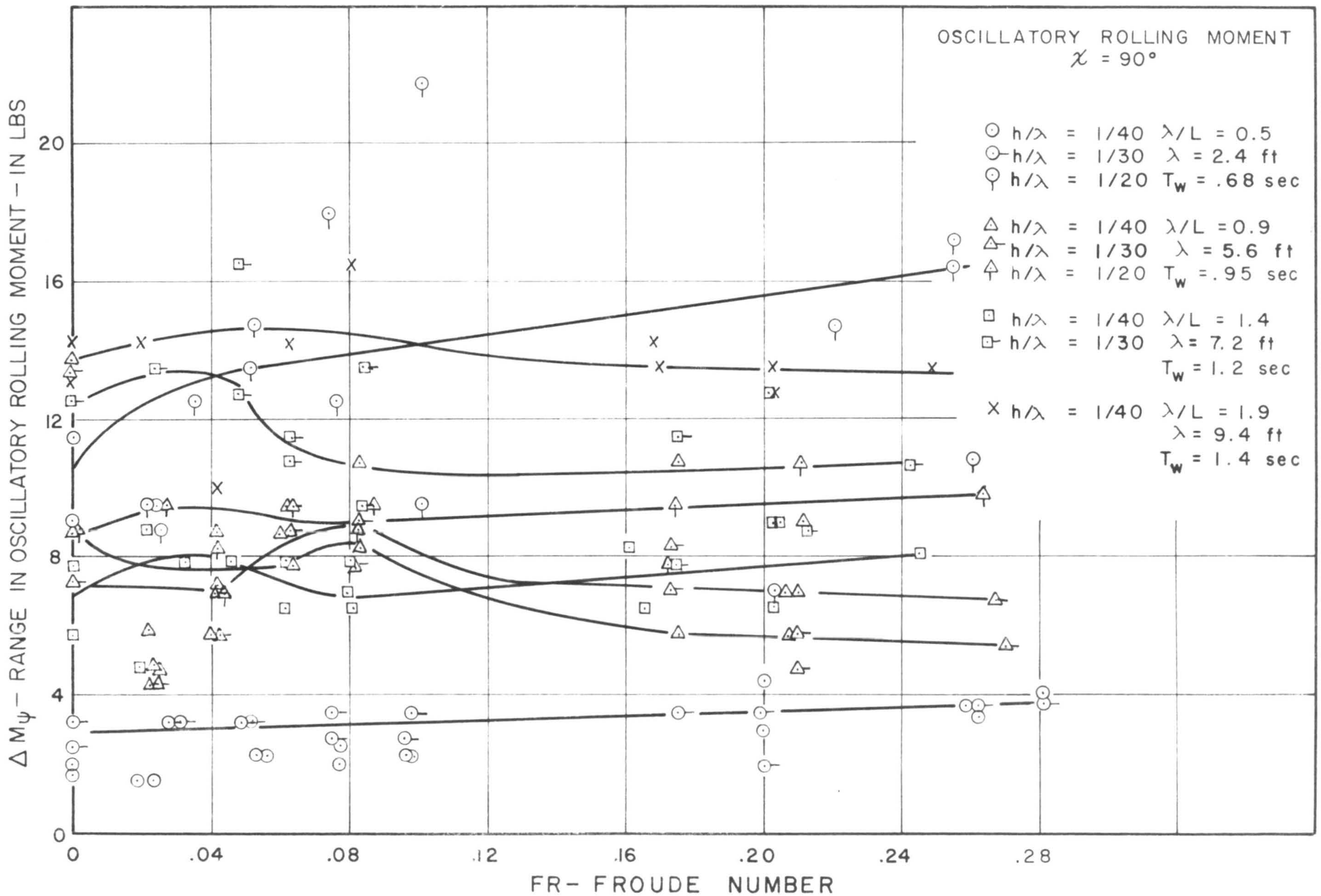

OSCILLATORY ROLLING MOMENT
χ = 90°
h/λ = 1/40 λ/L = 0.5
h/λ = 1/30 λ = 2.4 ft
h/λ = 1/20 T_w = .68 sec
h/λ = 1/40 λ/L = 0.9
h/λ = 1/30 λ = 5.6 ft
h/λ = 1/20 T_w = .95 sec
h/λ = 1/40 λ/L = 1.4
h/λ = 1/30 λ = 7.2 ft
T_w = 1.2 sec
X h/λ = 1/40 λ/L = 1.9
λ = 9.4 ft
T_w = 1.4 sec
ΔM_ψ – RANGE IN OSCILLATORY ROLLING MOMENT – IN LBS
0
4
8
12
16
20
0
.04
.08
.12
.16
.20
.24
.28
FR – FROUDE NUMBER

FIG. 17

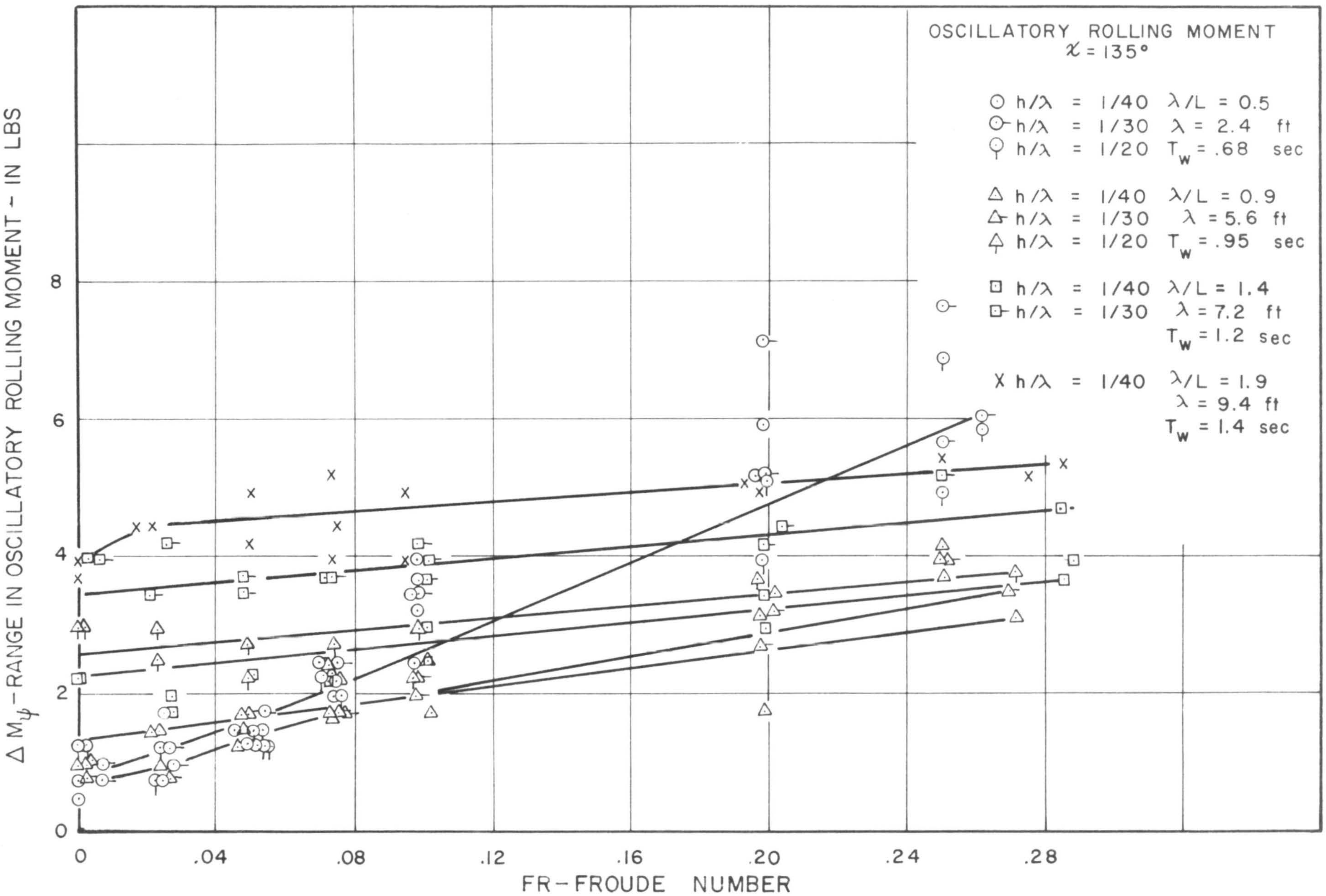

OSCILLATORY ROLLING MOMENT
$\chi = 135°$
h/λ = 1/40 λ/L = 0.5
h/λ = 1/30 λ = 2.4 ft
h/λ = 1/20 T_w = .68 sec
h/λ = 1/40 λ/L = 0.9
h/λ = 1/30 λ = 5.6 ft
h/λ = 1/20 T_w = .95 sec
h/λ = 1/40 λ/L = 1.4
h/λ = 1/30 λ = 7.2 ft
T_w = 1.2 sec
X h/λ = 1/40 λ/L = 1.9
λ = 9.4 ft
T_w = 1.4 sec
ΔM_ψ - RANGE IN OSCILLATORY ROLLING MOMENT - IN LBS
0
2
4
6
8
0
.04
.08
.12
.16
.20
.24
.28
FR - FROUDE NUMBER

FIG. 18

FIG. 18

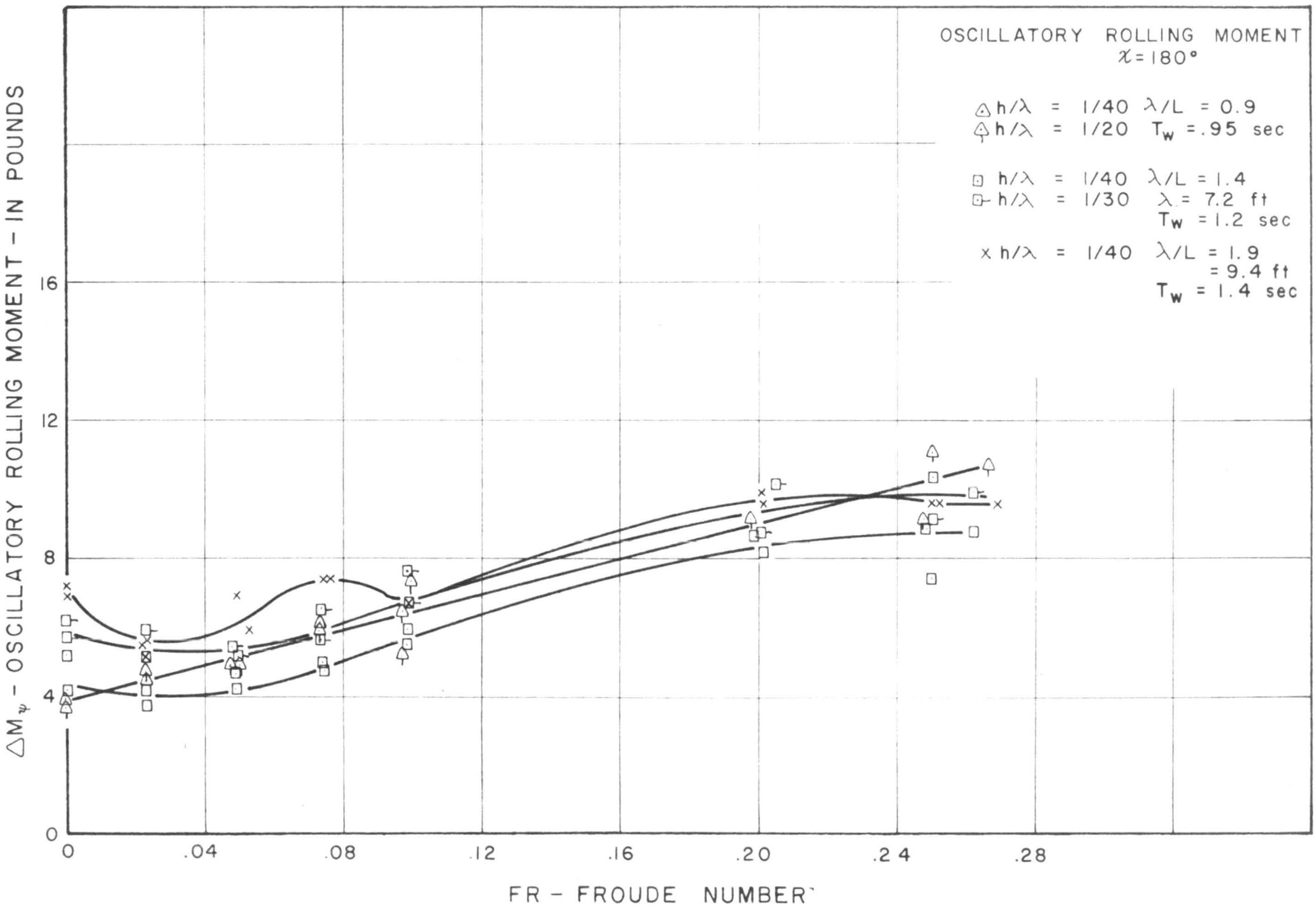
OSCILLATORY ROLLING MOMENT
χ = 180°
h/λ = 1/40 λ/L = 0.9
h/λ = 1/20 T_w = .95 sec
h/λ = 1/40 λ/L = 1.4
h/λ = 1/30 λ = 7.2 ft
T_w = 1.2 sec
× h/λ = 1/40 λ/L = 1.9
= 9.4 ft
T_w = 1.4 sec
ΔM_ψ - OSCILLATORY ROLLING MOMENT - IN POUNDS
FR - FROUDE NUMBER
0
4
8
12
16
.04
.08
.12
.16
.20
.24
.28

FIG. 19

FIG. 19

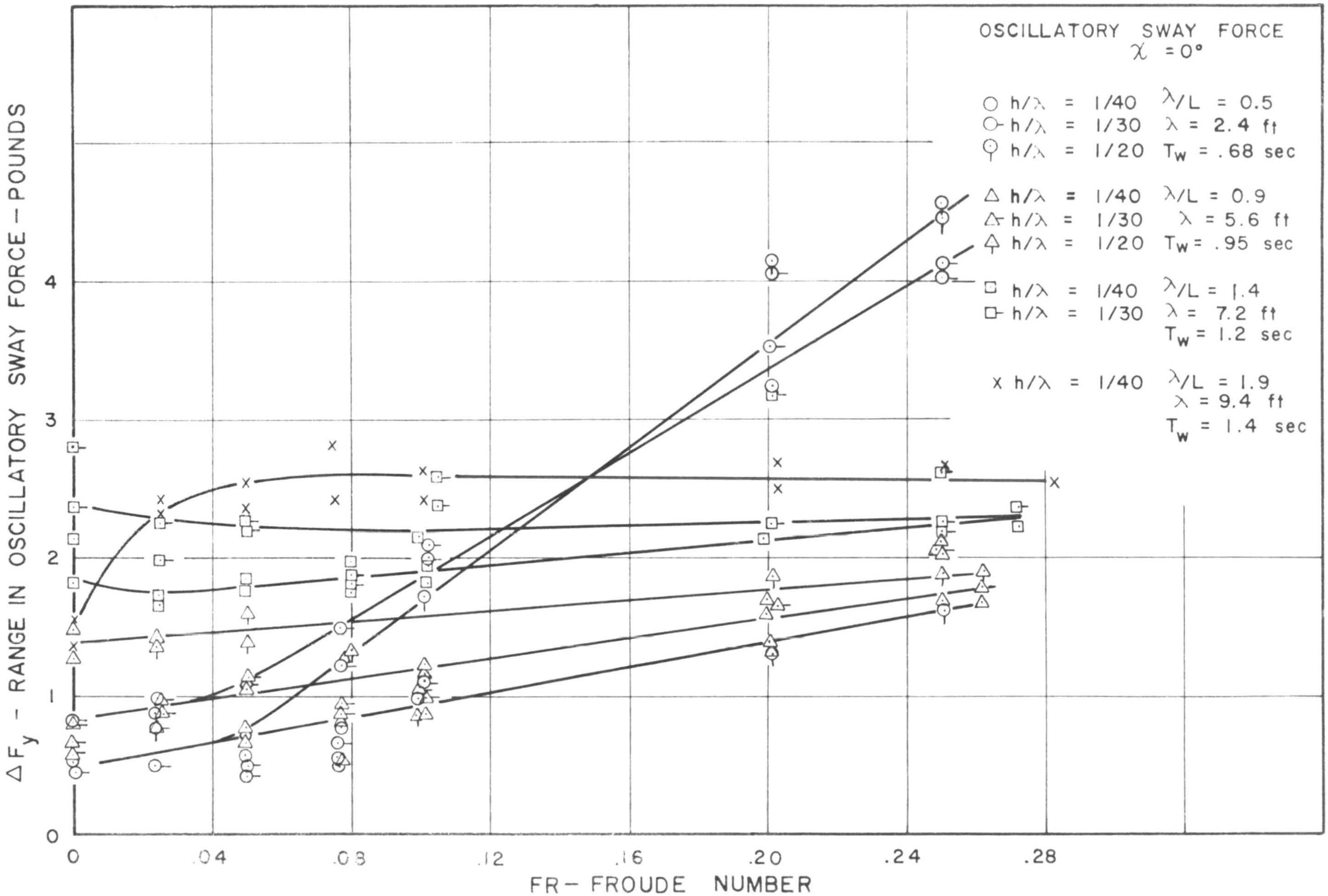

OSCILLATORY SWAY FORCE
χ = 0°
h/λ = 1/40 λ/L = 0.5
h/λ = 1/30 λ = 2.4 ft
h/λ = 1/20 Tw = .68 sec
h/λ = 1/40 λ/L = 0.9
h/λ = 1/30 λ = 5.6 ft
h/λ = 1/20 Tw = .95 sec
h/λ = 1/40 λ/L = 1.4
h/λ = 1/30 λ = 7.2 ft
Tw = 1.2 sec
x h/λ = 1/40 λ/L = 1.9
λ = 9.4 ft
Tw = 1.4 sec
ΔFy - RANGE IN OSCILLATORY SWAY FORCE - POUNDS
0
1
2
3
4
0
.04
.08
.12
.16
.20
.24
.28
FR - FROUDE NUMBER

FIG. 20

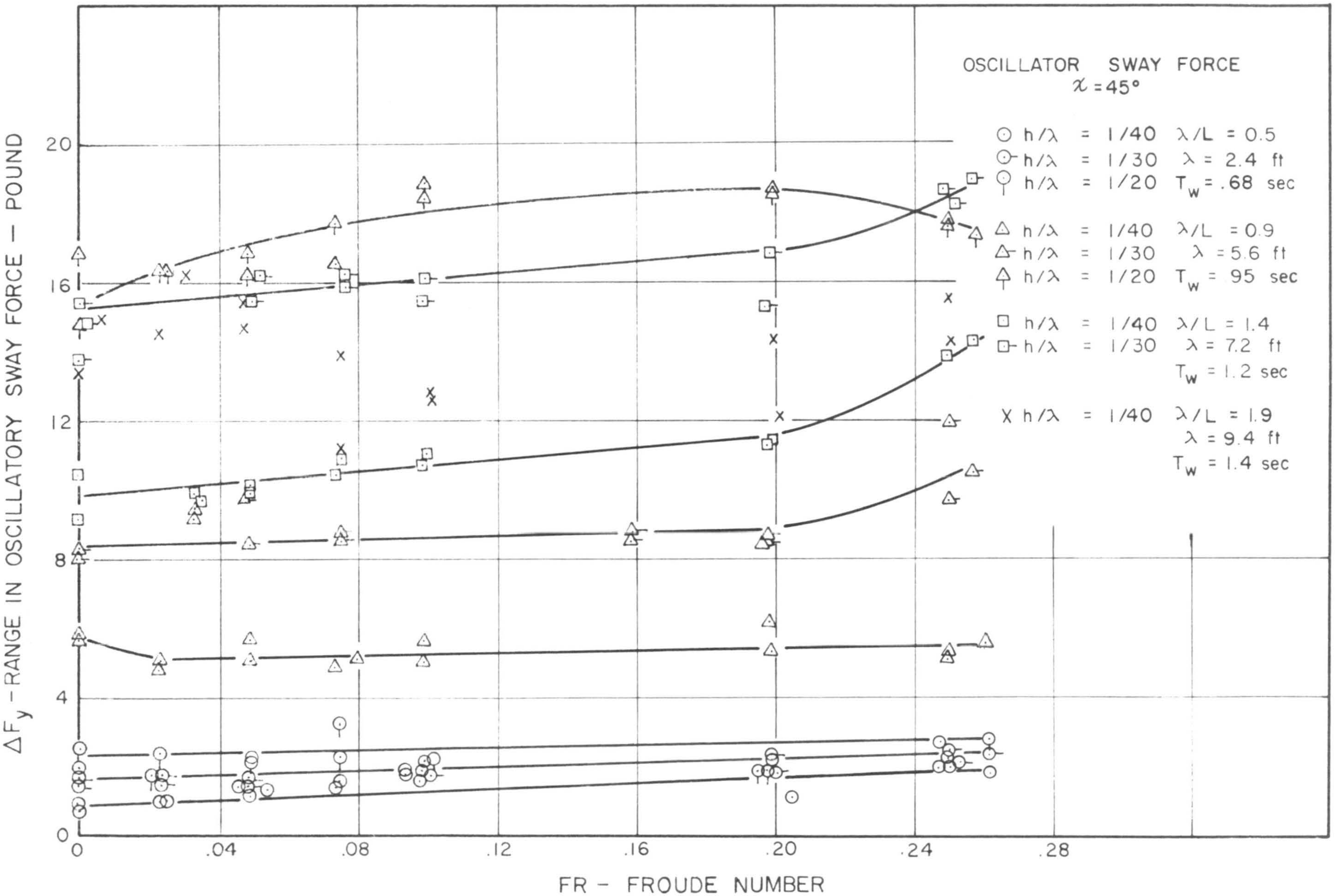

OSCILLATOR SWAY FORCE
χ = 45°
⊙ h/λ = 1/40 λ/L = 0.5
⊙ h/λ = 1/30 λ = 2.4 ft
⊙ h/λ = 1/20 T_W = .68 sec
△ h/λ = 1/40 λ/L = 0.9
△ h/λ = 1/30 λ = 5.6 ft
△ h/λ = 1/20 T_W = .95 sec
□ h/λ = 1/40 λ/L = 1.4
□ h/λ = 1/30 λ = 7.2 ft
T_W = 1.2 sec
X h/λ = 1/40 λ/L = 1.9
λ = 9.4 ft
T_W = 1.4 sec
ΔF_y - RANGE IN OSCILLATORY SWAY FORCE - POUND
FR - FROUDE NUMBER
0
4
8
12
16
20
0
.04
.08
.12
.16
.20
.24
.28

FIG. 21

FIG. 21

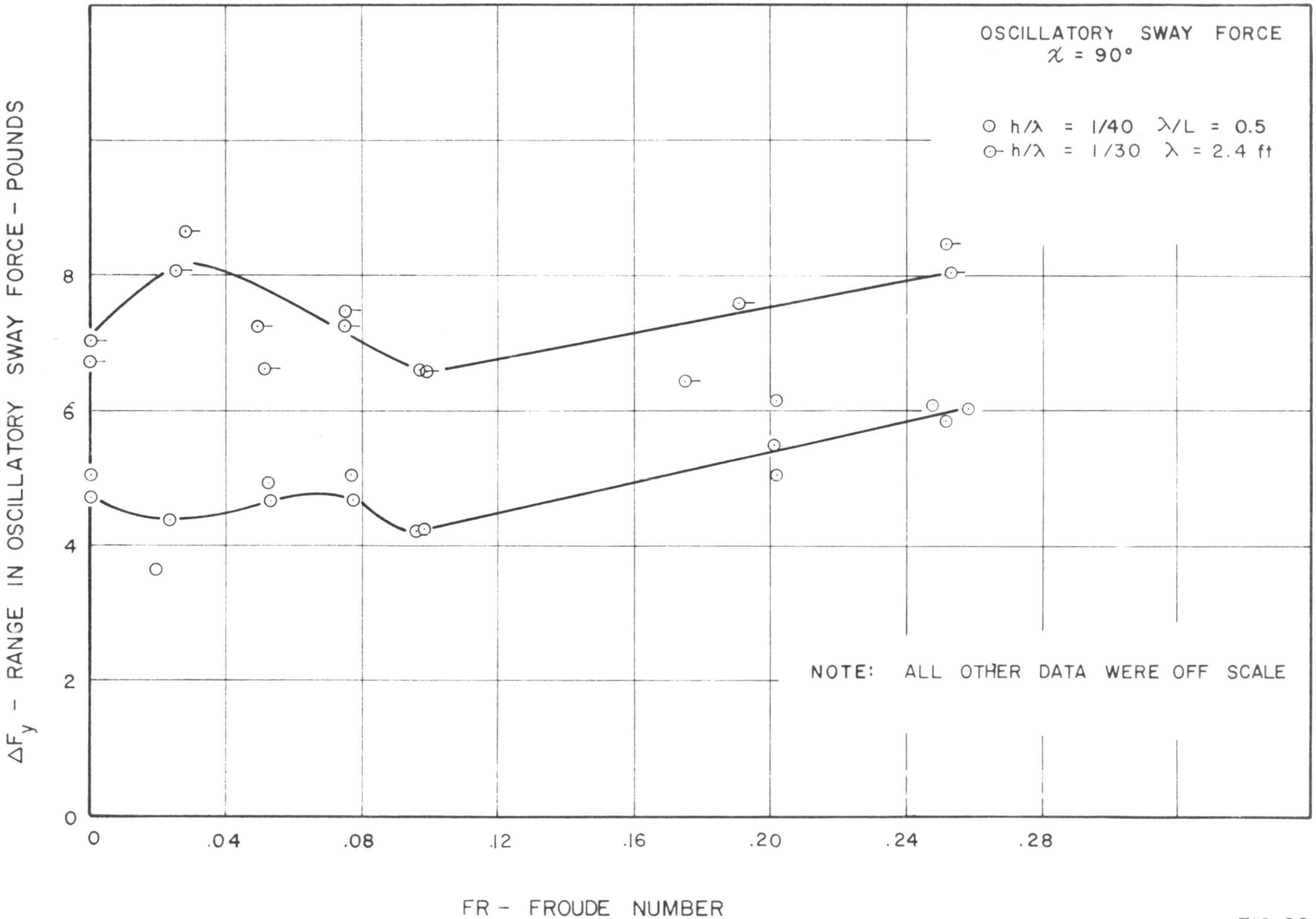

OSCILLATORY SWAY FORCE
χ = 90°
○ h/λ = 1/40 λ/L = 0.5
⊙- h/λ = 1/30 λ = 2.4 ft
NOTE: ALL OTHER DATA WERE OFF SCALE
ΔF_y - RANGE IN OSCILLATORY SWAY FORCE - POUNDS
FR - FROUDE NUMBER
0
2
4
6
8
0
.04
.08
.12
.16
.20
.24
.28

FIG. 22

FIG. 22

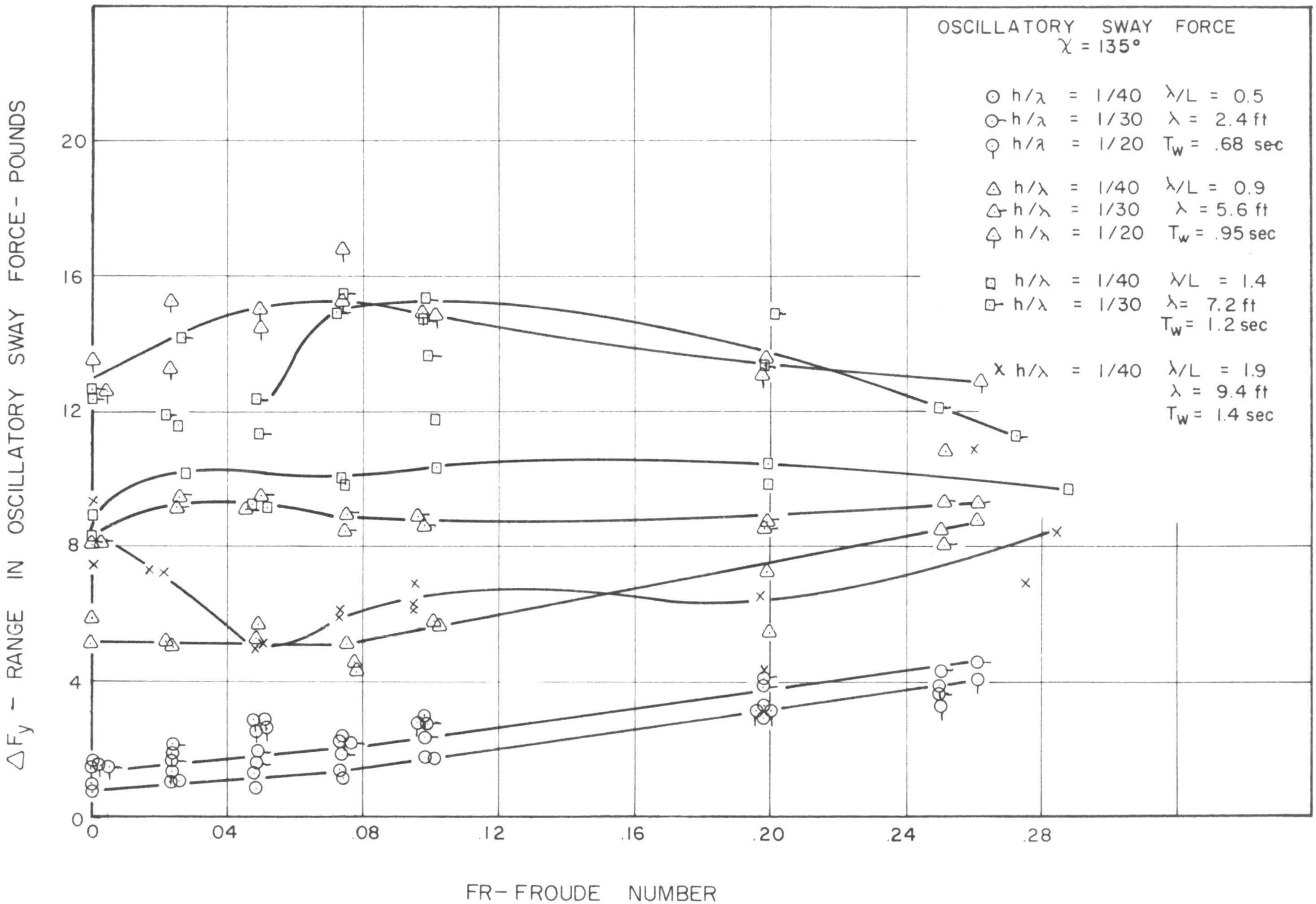
OSCILLATORY SWAY FORCE
χ = 135°
h/λ = 1/40 λ/L = 0.5
h/λ = 1/30 λ = 2.4 ft
h/λ = 1/20 Tw = .68 sec
h/λ = 1/40 λ/L = 0.9
h/λ = 1/30 λ = 5.6 ft
h/λ = 1/20 Tw = .95 sec
h/λ = 1/40 λ/L = 1.4
h/λ = 1/30 λ = 7.2 ft
Tw = 1.2 sec
X h/λ = 1/40 λ/L = 1.9
λ = 9.4 ft
Tw = 1.4 sec
ΔFy - RANGE IN OSCILLATORY SWAY FORCE - POUNDS
FR - FROUDE NUMBER
0
4
8
12
16
20
.04
.08
.12
.16
.20
.24
.28

FIG. 23

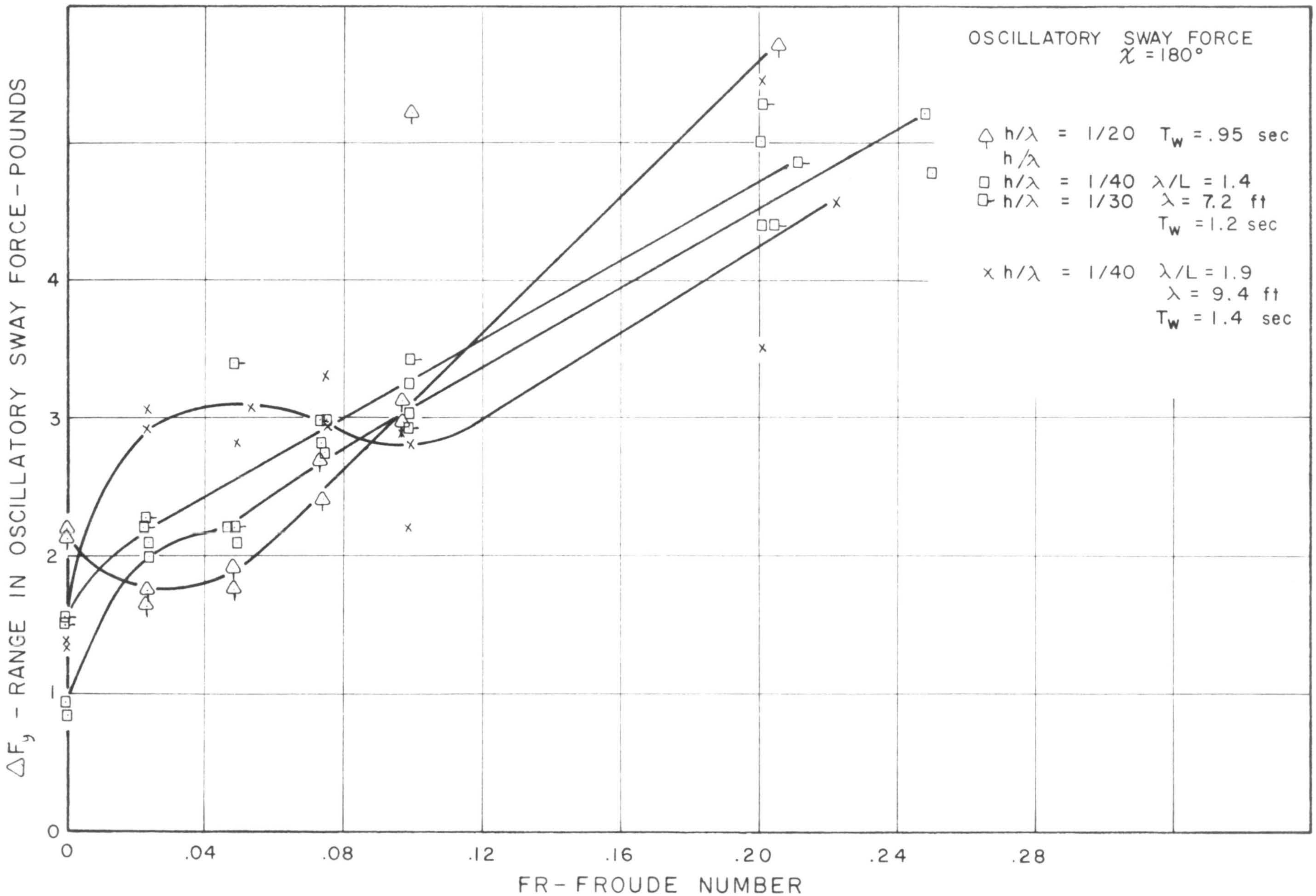

OSCILLATORY SWAY FORCE
χ = 180°
h/λ = 1/20 T_W = .95 sec
h/λ
h/λ = 1/40 λ/L = 1.4
h/λ = 1/30 λ = 7.2 ft
T_W = 1.2 sec
h/λ = 1/40 λ/L = 1.9
λ = 9.4 ft
T_W = 1.4 sec
ΔF_y - RANGE IN OSCILLATORY SWAY FORCE - POUNDS
FR - FROUDE NUMBER
0
1
2
3
4
0
.04
.08
.12
.16
.20
.24
.28

FIG. 24

FIG. 24

FIG. 25

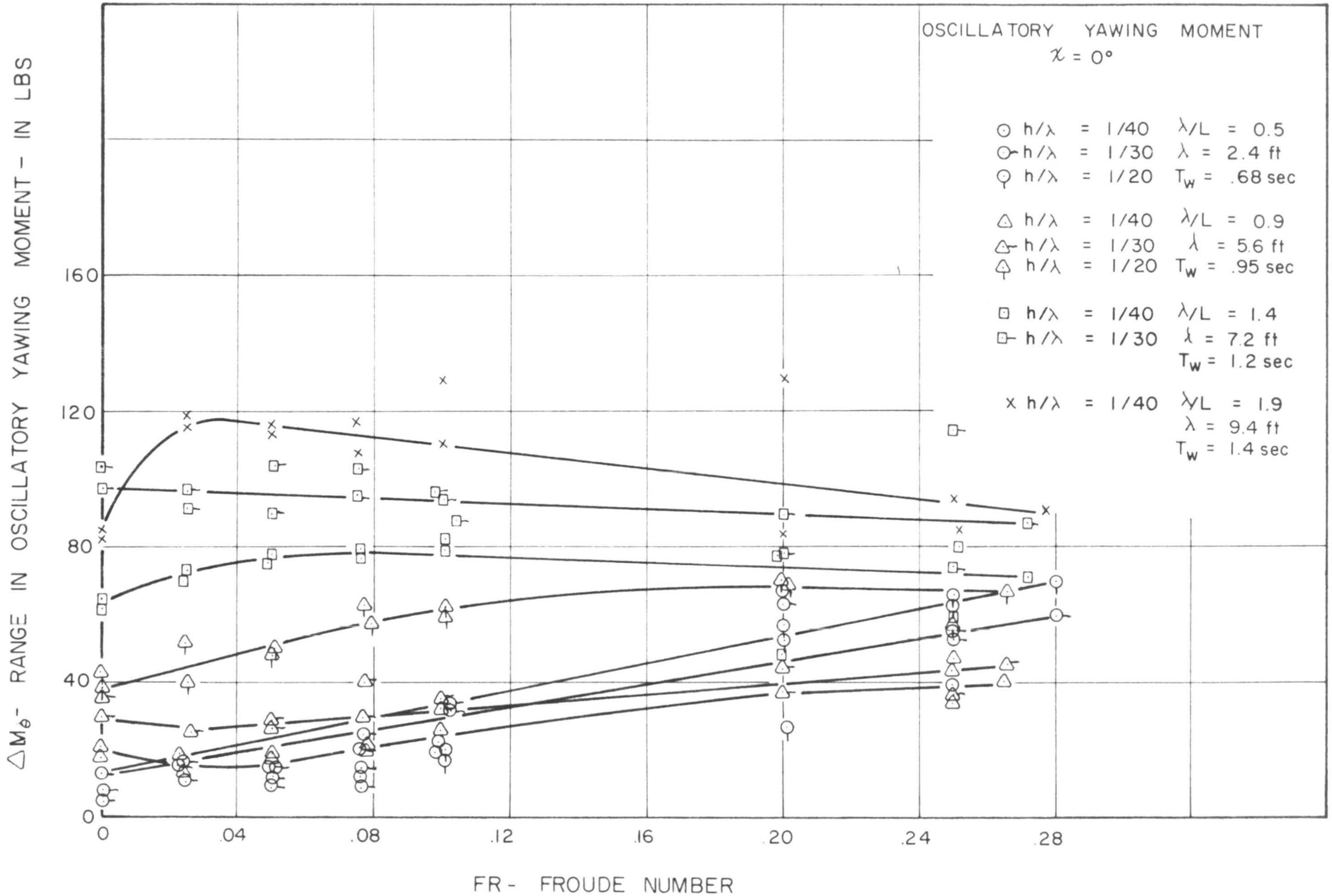
OSCILLATORY YAWING MOMENT
χ = 0°
h/λ = 1/40 λ/L = 0.5
h/λ = 1/30 λ = 2.4 ft
h/λ = 1/20 T_W = .68 sec
h/λ = 1/40 λ/L = 0.9
h/λ = 1/30 λ = 5.6 ft
h/λ = 1/20 T_W = .95 sec
h/λ = 1/40 λ/L = 1.4
h/λ = 1/30 λ = 7.2 ft
T_W = 1.2 sec
x h/λ = 1/40 λ/L = 1.9
λ = 9.4 ft
T_W = 1.4 sec
ΔM_ϕ - RANGE IN OSCILLATORY YAWING MOMENT - IN LBS
0
40
80
120
160
0
.04
.08
.12
.16
.20
.24
.28
FR - FROUDE NUMBER

FIG. 25

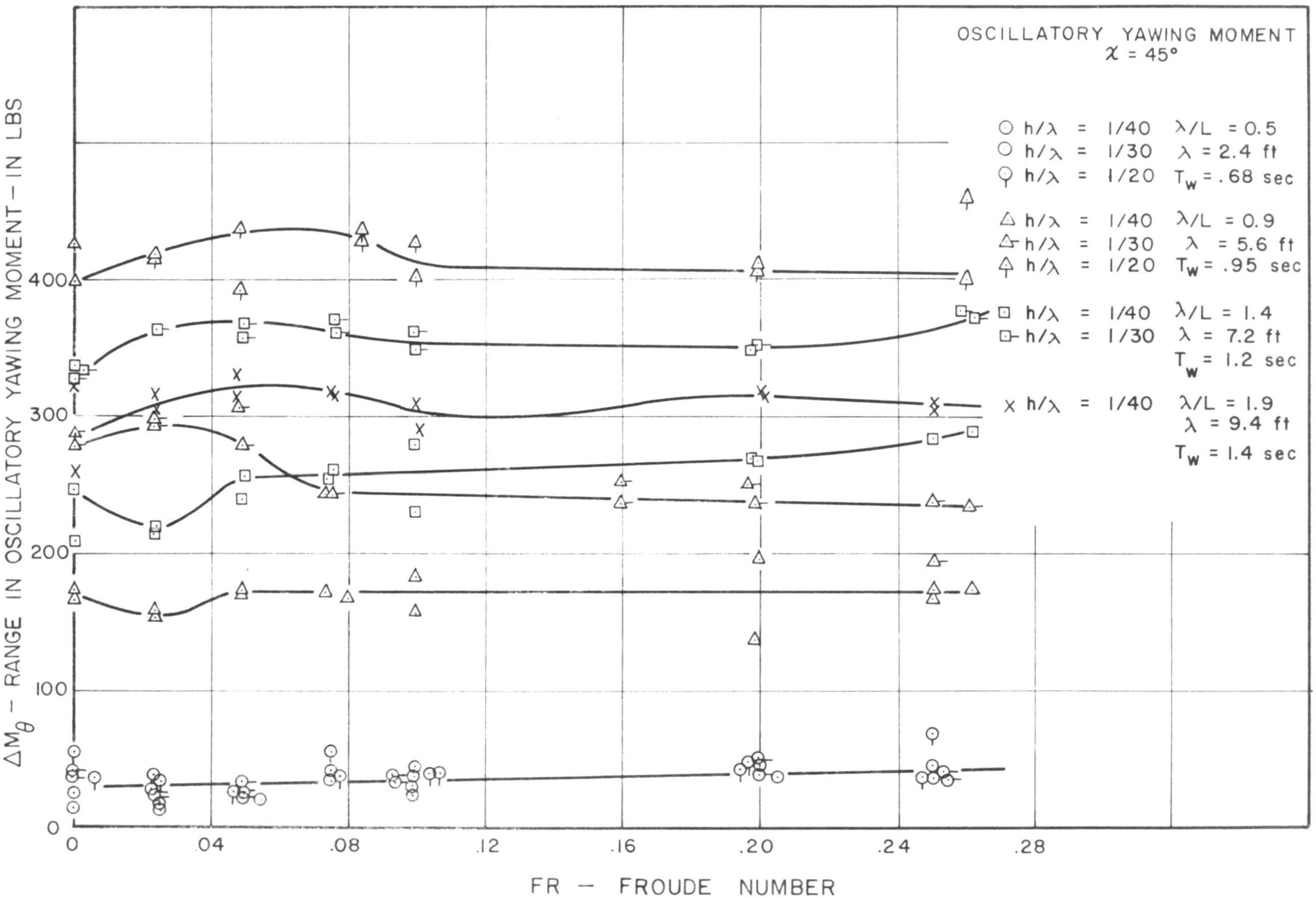

OSCILLATORY YAWING MOMENT
χ = 45°
○ h/λ = 1/40 λ/L = 0.5
○ h/λ = 1/30 λ = 2.4 ft
○ h/λ = 1/20 T_w = .68 sec
△ h/λ = 1/40 λ/L = 0.9
△ h/λ = 1/30 λ = 5.6 ft
△ h/λ = 1/20 T_w = .95 sec
□ h/λ = 1/40 λ/L = 1.4
□ h/λ = 1/30 λ = 7.2 ft
T_w = 1.2 sec
x h/λ = 1/40 λ/L = 1.9
λ = 9.4 ft
T_w = 1.4 sec
ΔM_θ - RANGE IN OSCILLATORY YAWING MOMENT - IN LBS
0
100
200
300
400
0
.04
.08
.12
.16
.20
.24
.28
FR — FROUDE NUMBER

FIG. 26

FIG. 26

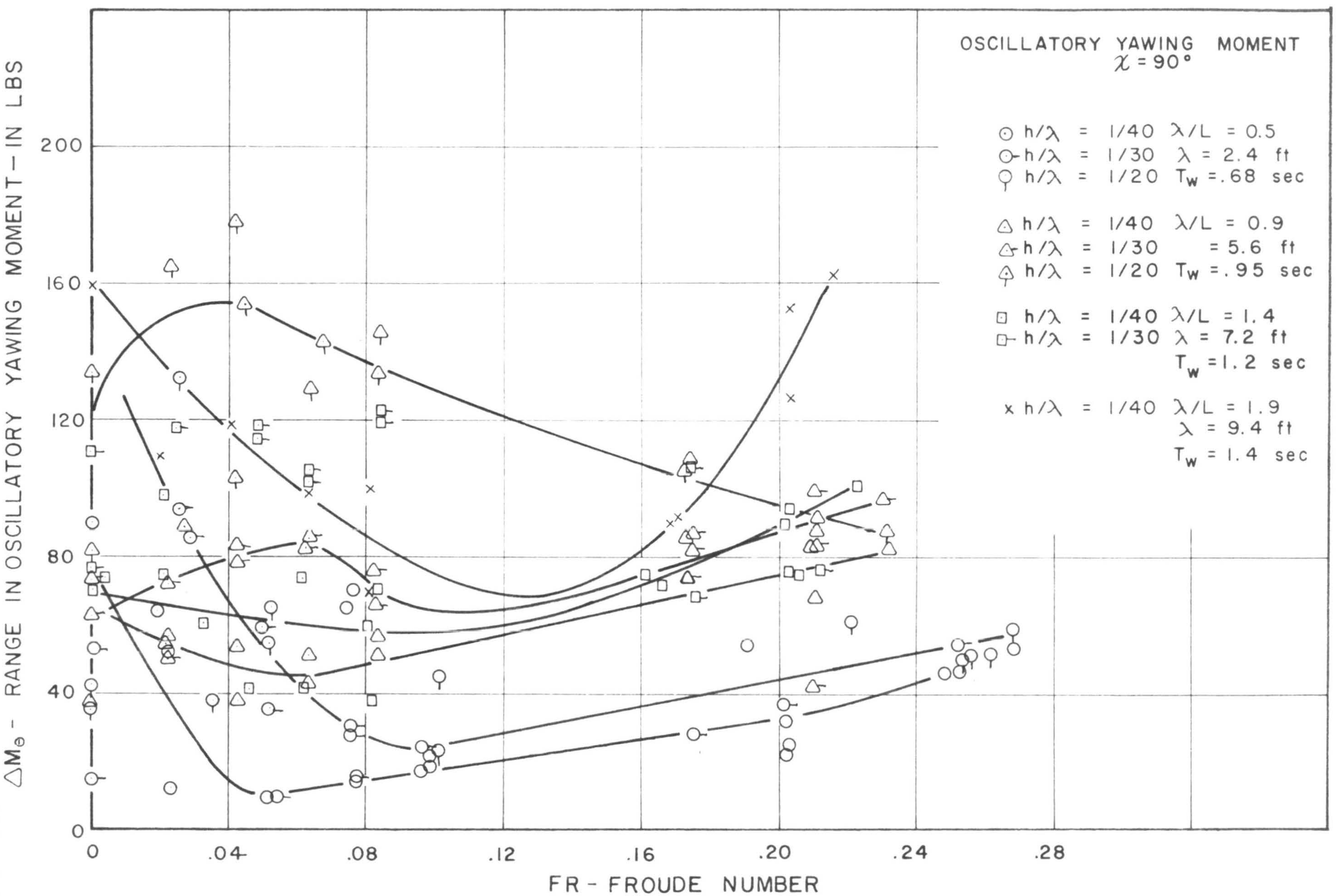

OSCILLATORY YAWING MOMENT
χ = 90°
⊙ h/λ = 1/40 λ/L = 0.5
○- h/λ = 1/30 λ = 2.4 ft
♀ h/λ = 1/20 Tw = .68 sec
△ h/λ = 1/40 λ/L = 0.9
△- h/λ = 1/30 = 5.6 ft
△ h/λ = 1/20 Tw = .95 sec
⊡ h/λ = 1/40 λ/L = 1.4
□- h/λ = 1/30 λ = 7.2 ft
Tw = 1.2 sec
× h/λ = 1/40 λ/L = 1.9
λ = 9.4 ft
Tw = 1.4 sec
ΔMθ - RANGE IN OSCILLATORY YAWING MOMENT - IN LBS
0
40
80
120
160
200
0
.04
.08
.12
.16
.20
.24
.28
FR - FROUDE NUMBER

FIG. 27

FIG. 27

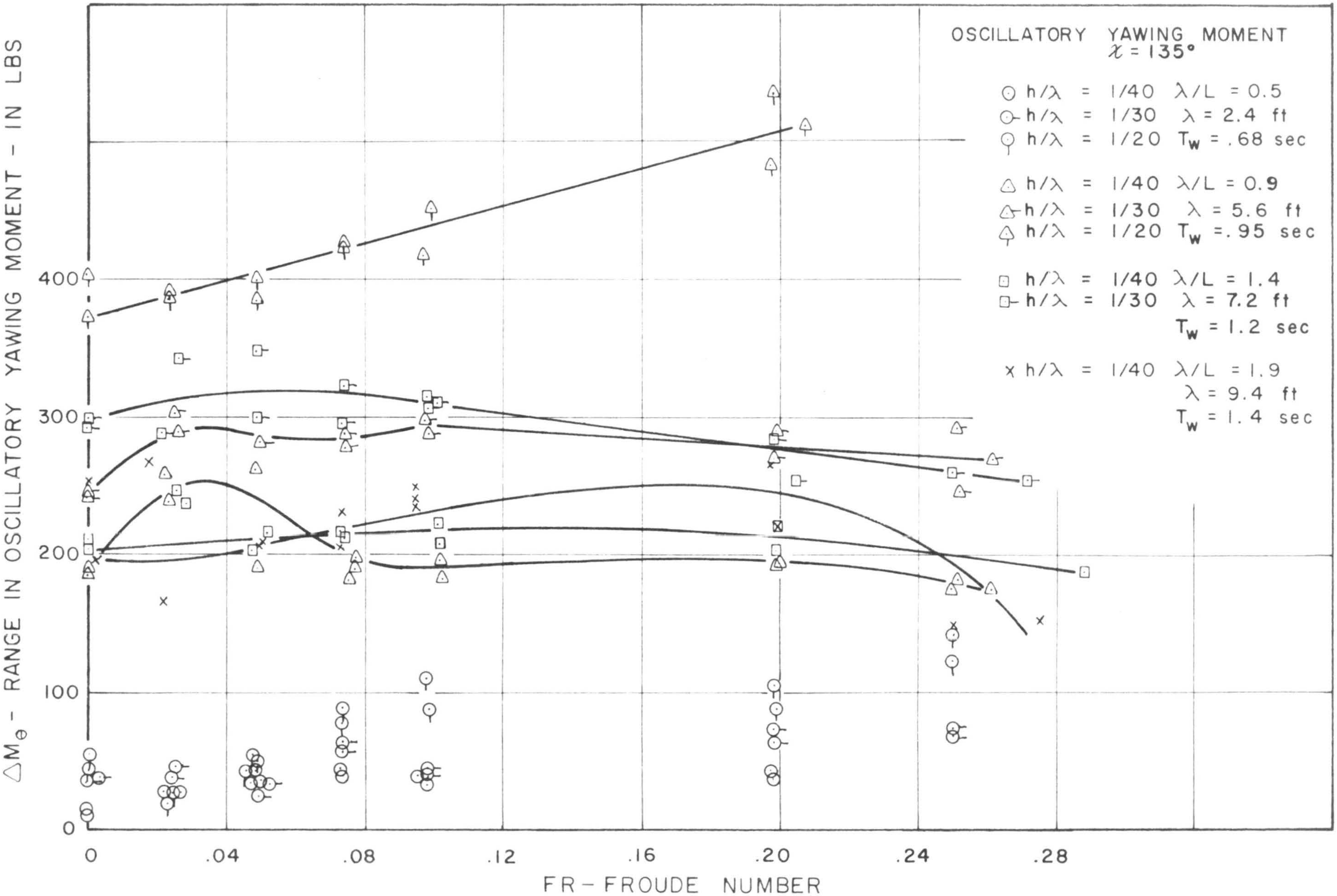

OSCILLATORY YAWING MOMENT
χ = 135°
h/λ = 1/40 λ/L = 0.5
h/λ = 1/30 λ = 2.4 ft
h/λ = 1/20 T_W = .68 sec
h/λ = 1/40 λ/L = 0.9
h/λ = 1/30 λ = 5.6 ft
h/λ = 1/20 T_W =.95 sec
h/λ = 1/40 λ/L = 1.4
h/λ = 1/30 λ = 7.2 ft
T_W = 1.2 sec
x h/λ = 1/40 λ/L = 1.9
λ = 9.4 ft
T_W = 1.4 sec
ΔMθ - RANGE IN OSCILLATORY YAWING MOMENT - IN LBS
0
100
200
300
400
0
.04
.08
.12
.16
.20
.24
.28
FR - FROUDE NUMBER

FIG. 28

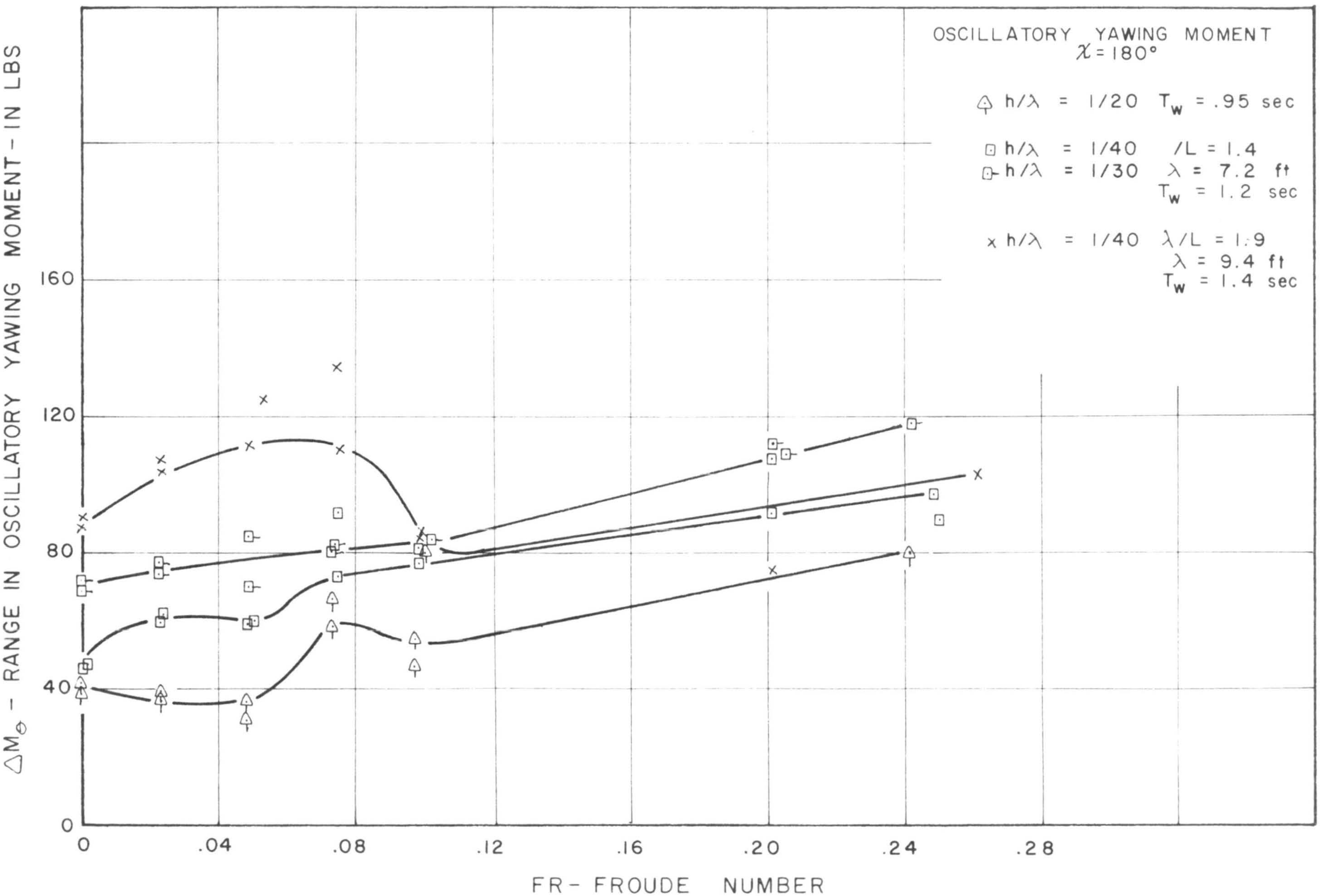

OSCILLATORY YAWING MOMENT
χ = 180°
h/λ = 1/20 T_w = .95 sec
h/λ = 1/40 /L = 1.4
h/λ = 1/30 λ = 7.2 ft
T_w = 1.2 sec
h/λ = 1/40 λ/L = 1.9
λ = 9.4 ft
T_w = 1.4 sec
ΔM$_\phi$ - RANGE IN OSCILLATORY YAWING MOMENT - IN LBS
0
40
80
120
160
0
.04
.08
.12
.16
.20
.24
.28
FR - FROUDE NUMBER

FIG. 29

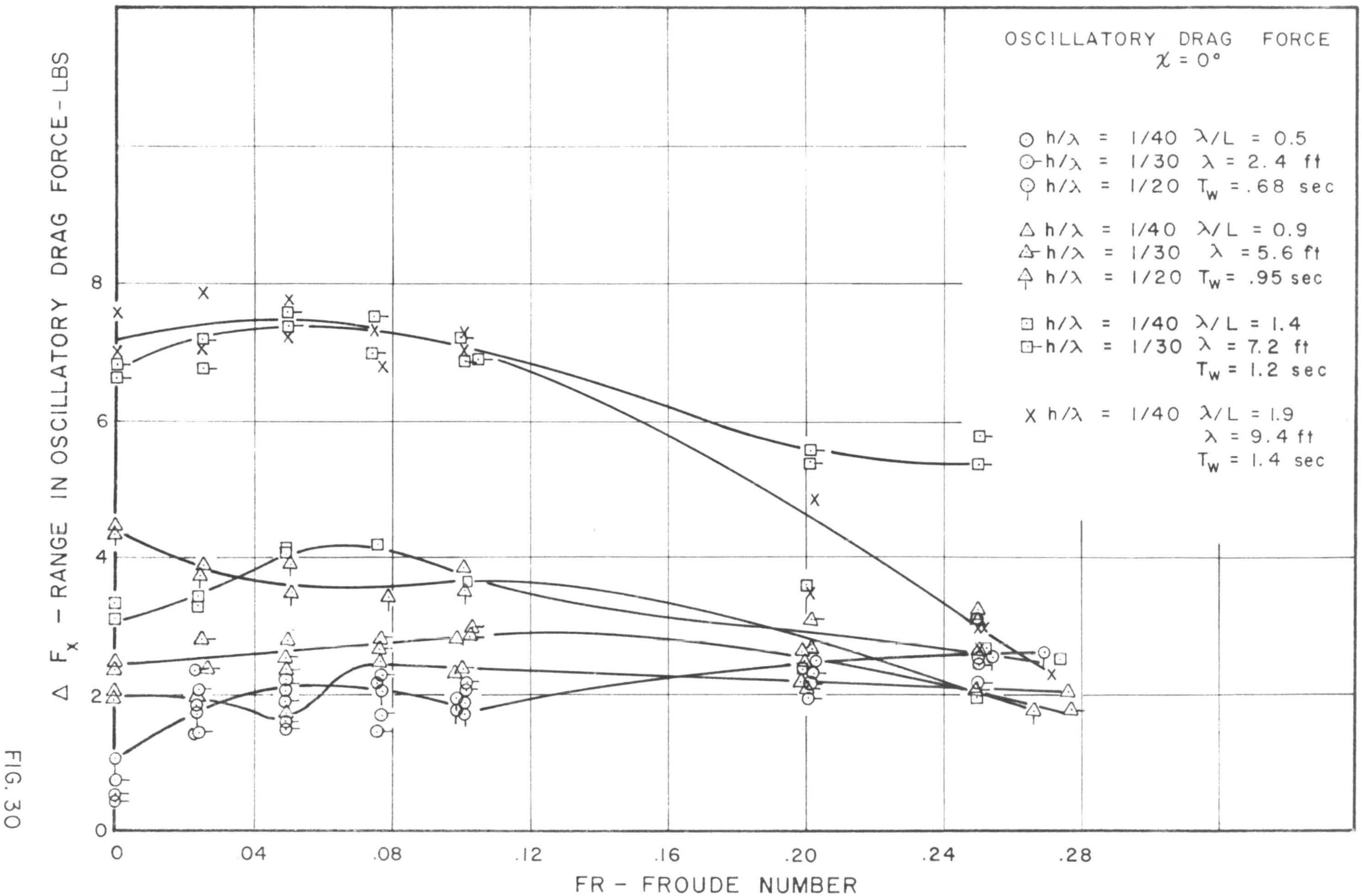
OSCILLATORY DRAG FORCE
χ = 0°
⊙ h/λ = 1/40 λ/L = 0.5
⊙- h/λ = 1/30 λ = 2.4 ft
⊙ h/λ = 1/20 T_W = .68 sec
△ h/λ = 1/40 λ/L = 0.9
△- h/λ = 1/30 λ = 5.6 ft
△ h/λ = 1/20 T_W = .95 sec
⊡ h/λ = 1/40 λ/L = 1.4
⊡- h/λ = 1/30 λ = 7.2 ft
T_W = 1.2 sec
X h/λ = 1/40 λ/L = 1.9
λ = 9.4 ft
T_W = 1.4 sec
ΔF_x - RANGE IN OSCILLATORY DRAG FORCE - LBS
0
2
4
6
8
0
.04
.08
.12
.16
.20
.24
.28
FR - FROUDE NUMBER
FIG. 30

FIG. 30

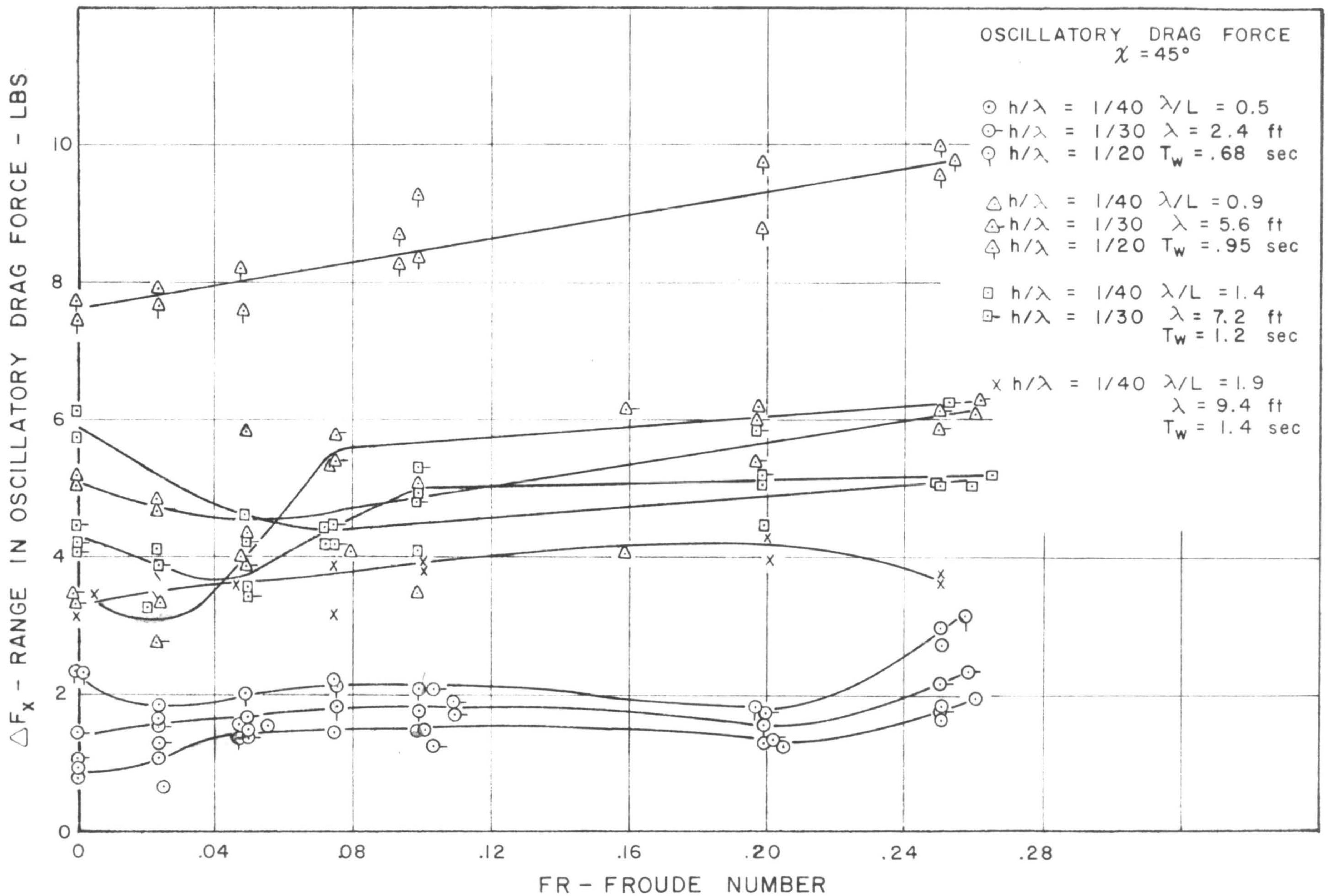

OSCILLATORY DRAG FORCE
χ = 45°
h/λ = 1/40 λ/L = 0.5
h/λ = 1/30 λ = 2.4 ft
h/λ = 1/20 T_w = .68 sec
h/λ = 1/40 λ/L = 0.9
h/λ = 1/30 λ = 5.6 ft
h/λ = 1/20 T_w = .95 sec
h/λ = 1/40 λ/L = 1.4
h/λ = 1/30 λ = 7.2 ft
T_w = 1.2 sec
x h/λ = 1/40 λ/L = 1.9
λ = 9.4 ft
T_w = 1.4 sec
ΔF_x - RANGE IN OSCILLATORY DRAG FORCE - LBS
FR - FROUDE NUMBER
0
2
4
6
8
10
.04
.08
.12
.16
.20
.24
.28

FIG. 31

FIG. 31

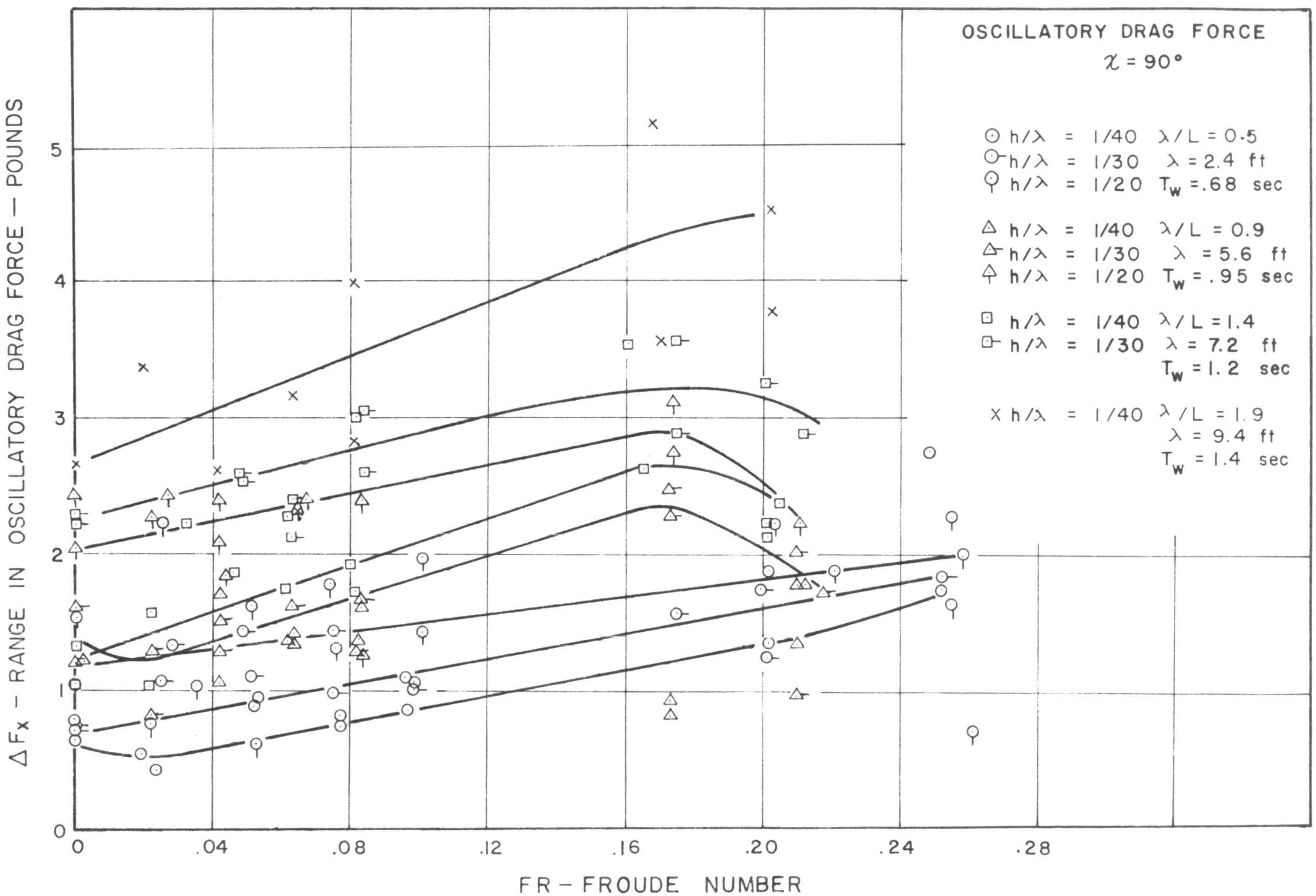
OSCILLATORY DRAG FORCE
$\chi = 90°$
h/λ = 1/40 λ/L = 0.5
h/λ = 1/30 λ = 2.4 ft
h/λ = 1/20 T_w = .68 sec
h/λ = 1/40 λ/L = 0.9
h/λ = 1/30 λ = 5.6 ft
h/λ = 1/20 T_w = .95 sec
h/λ = 1/40 λ/L = 1.4
h/λ = 1/30 λ = 7.2 ft
T_w = 1.2 sec
X h/λ = 1/40 λ/L = 1.9
λ = 9.4 ft
T_w = 1.4 sec
ΔF_x - RANGE IN OSCILLATORY DRAG FORCE — POUNDS
FR – FROUDE NUMBER
0
.04
.08
.12
.16
.20
.24
.28
1
2
3
4
5

FIG. 32

FIG. 32

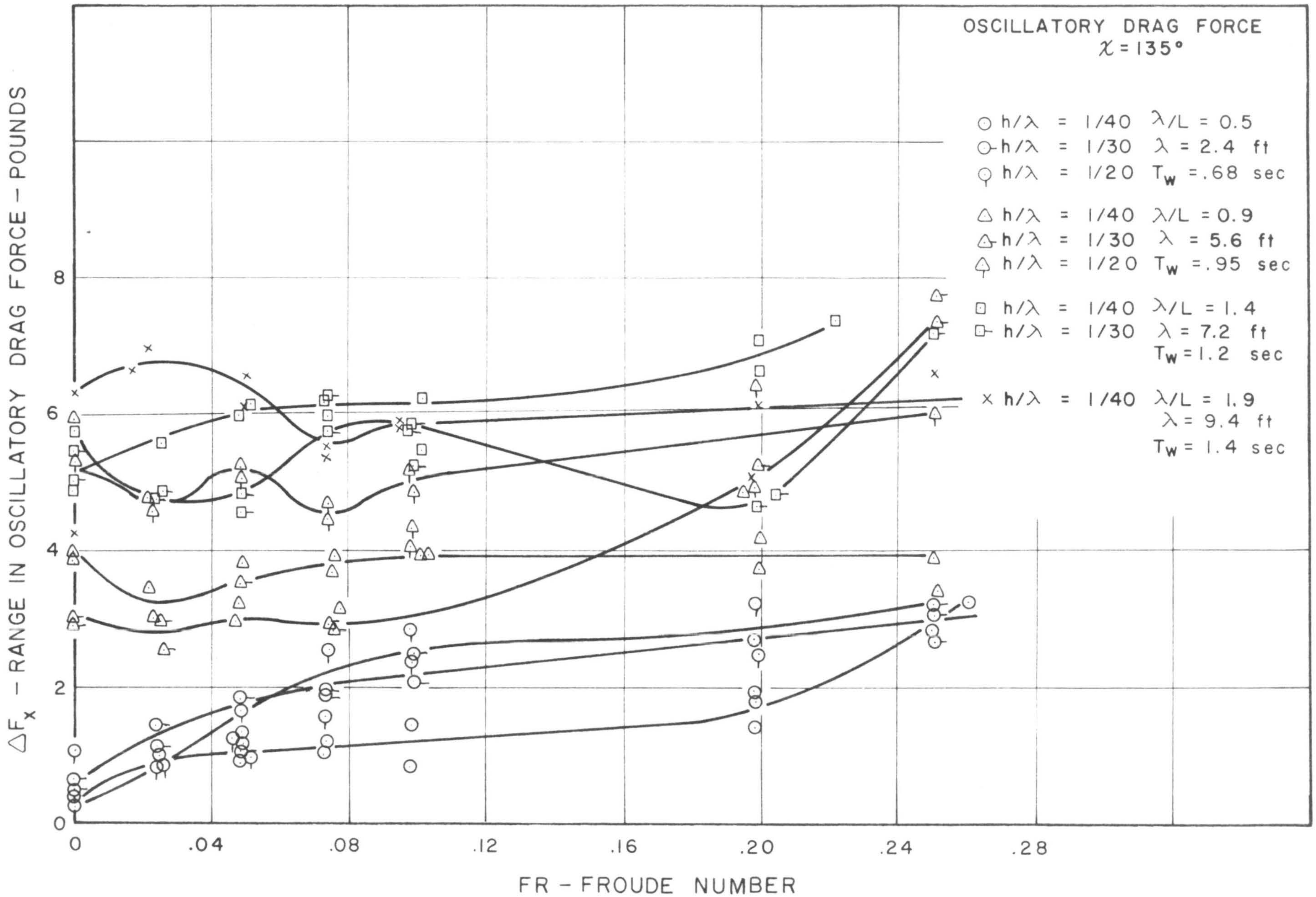

OSCILLATORY DRAG FORCE
χ = 135°
h/λ = 1/40 λ/L = 0.5
h/λ = 1/30 λ = 2.4 ft
h/λ = 1/20 Tw = .68 sec
h/λ = 1/40 λ/L = 0.9
h/λ = 1/30 λ = 5.6 ft
h/λ = 1/20 Tw = .95 sec
h/λ = 1/40 λ/L = 1.4
h/λ = 1/30 λ = 7.2 ft
Tw = 1.2 sec
× h/λ = 1/40 λ/L = 1.9
λ = 9.4 ft
Tw = 1.4 sec
ΔFx - RANGE IN OSCILLATORY DRAG FORCE - POUNDS
0
2
4
6
8
0
.04
.08
.12
.16
.20
.24
.28
FR - FROUDE NUMBER

FIG. 33

FIG. 33

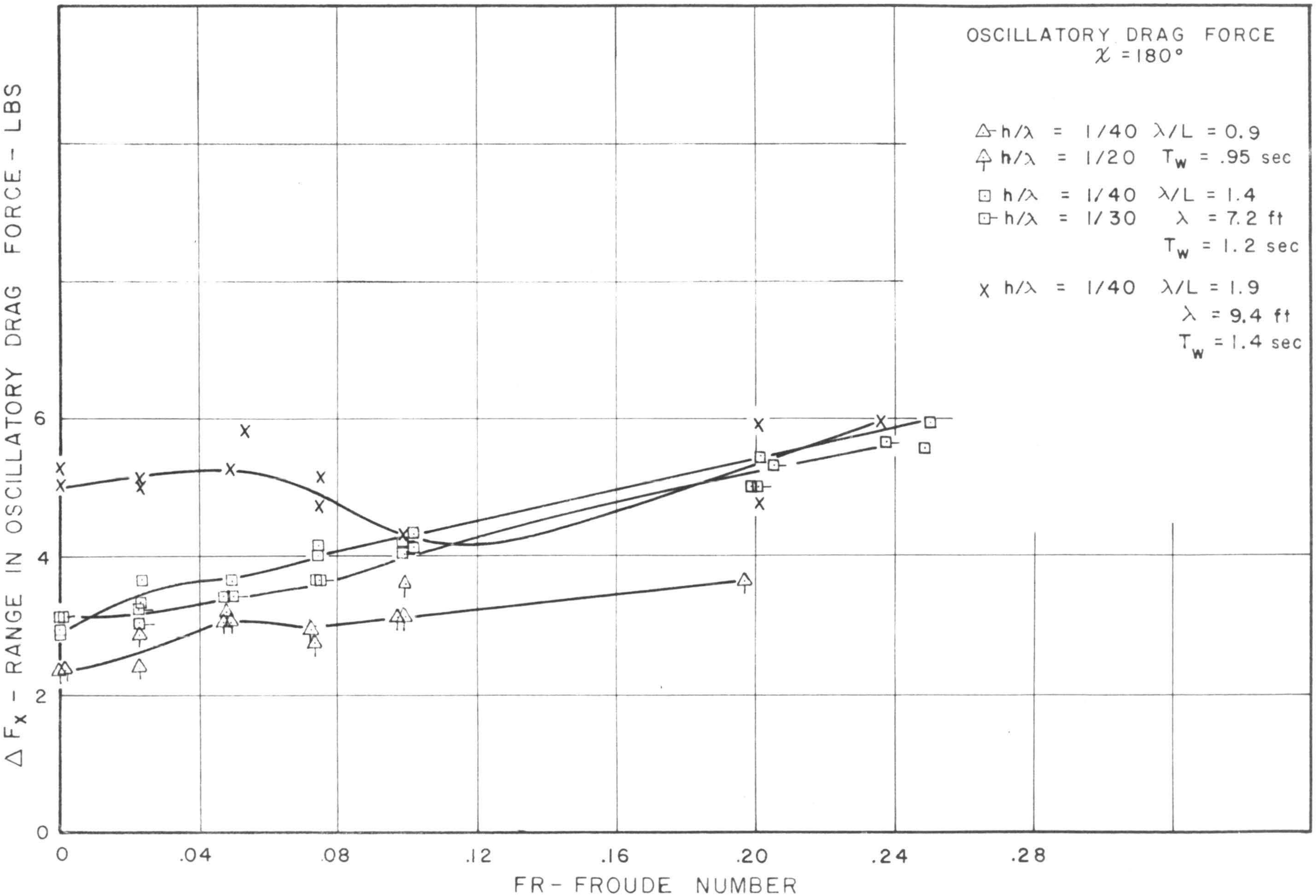

OSCILLATORY DRAG FORCE
χ = 180°
h/λ = 1/40 λ/L = 0.9
h/λ = 1/20 T_W = .95 sec
h/λ = 1/40 λ/L = 1.4
h/λ = 1/30 λ = 7.2 ft
T_W = 1.2 sec
h/λ = 1/40 λ/L = 1.9
λ = 9.4 ft
T_W = 1.4 sec
ΔF$_x$ - RANGE IN OSCILLATORY DRAG FORCE - LBS
0
2
4
6
0
.04
.08
.12
.16
.20
.24
.28
FR - FROUDE NUMBER

FIG. 34

FIG. 34

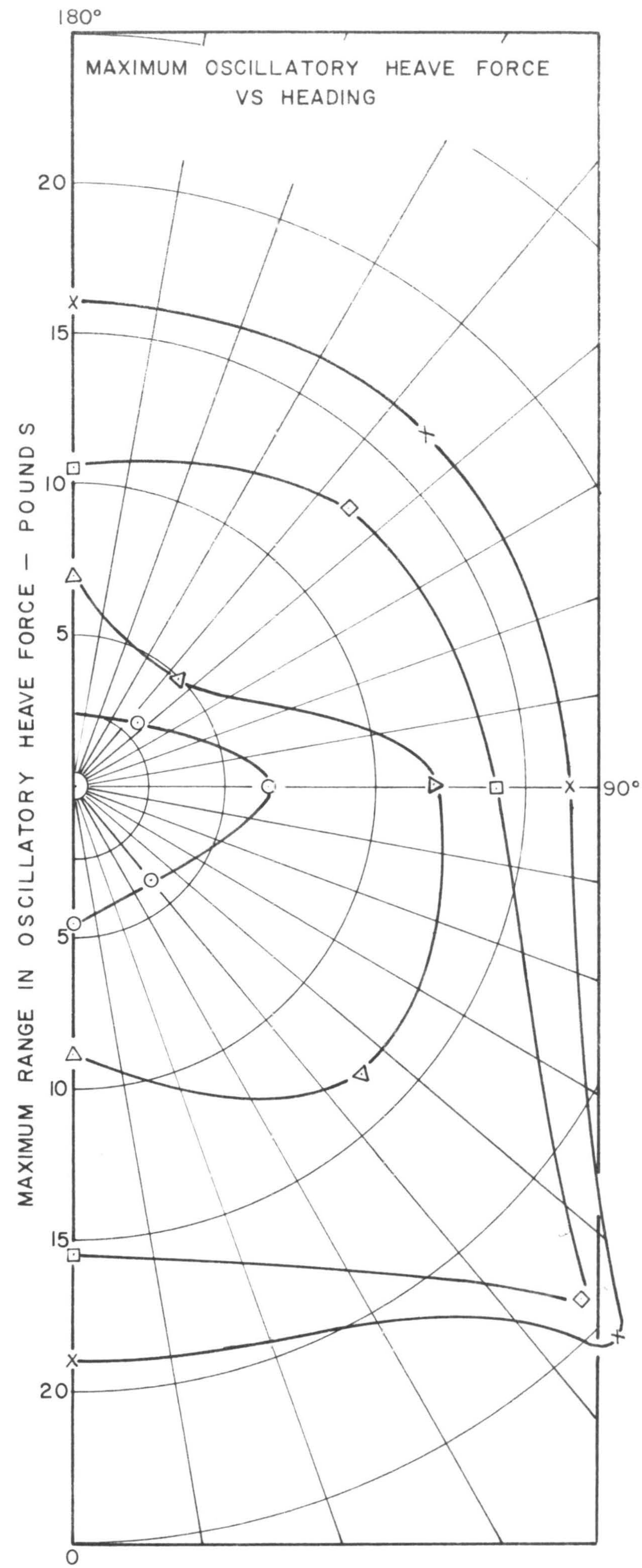
180°
MAXIMUM OSCILLATORY HEAVE FORCE
VS HEADING
MAXIMUM RANGE IN OSCILLATORY HEAVE FORCE — POUNDS
20
15
10
5
5
10
15
20
0
90°

FIG. 35

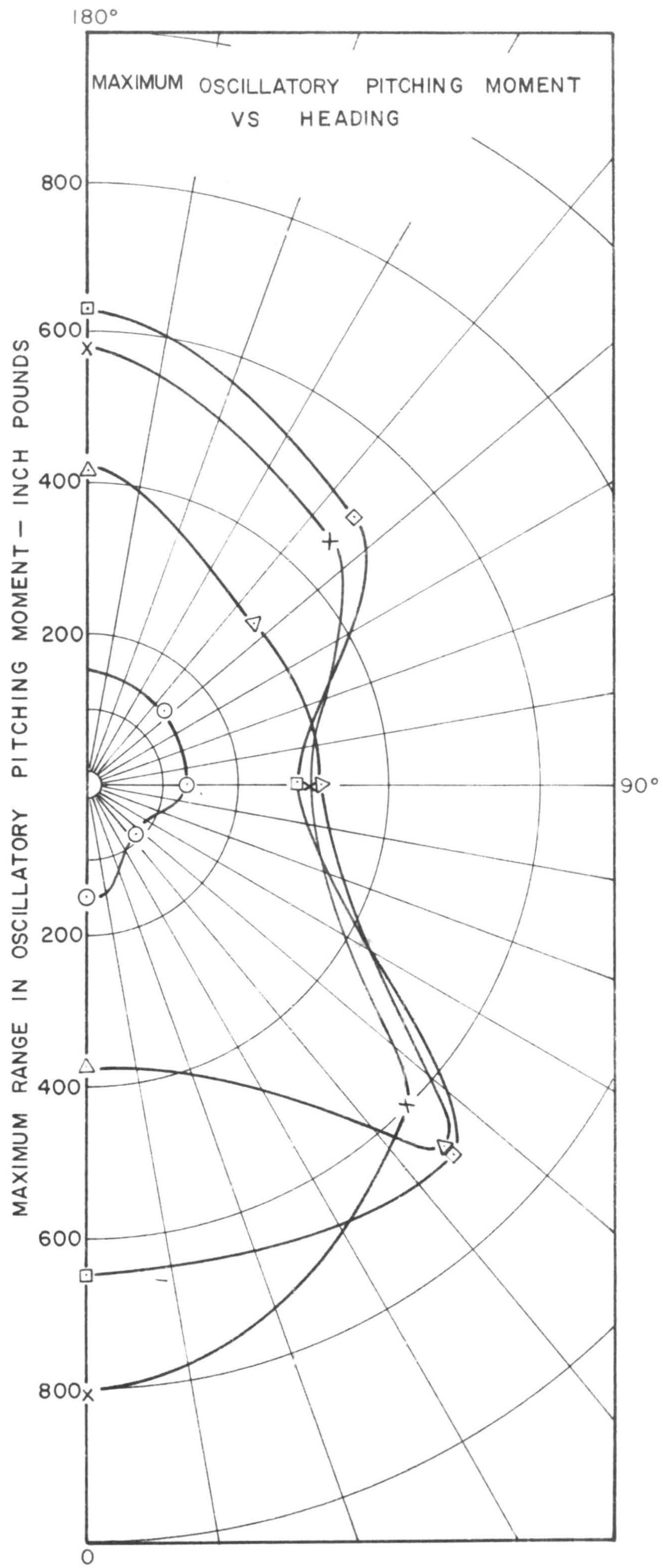

MAXIMUM OSCILLATORY PITCHING MOMENT
VS HEADING
MAXIMUM RANGE IN OSCILLATORY PITCHING MOMENT — INCH POUNDS
180°
800
600
400
200
200
400
600
800
90°
0

FIG. 36

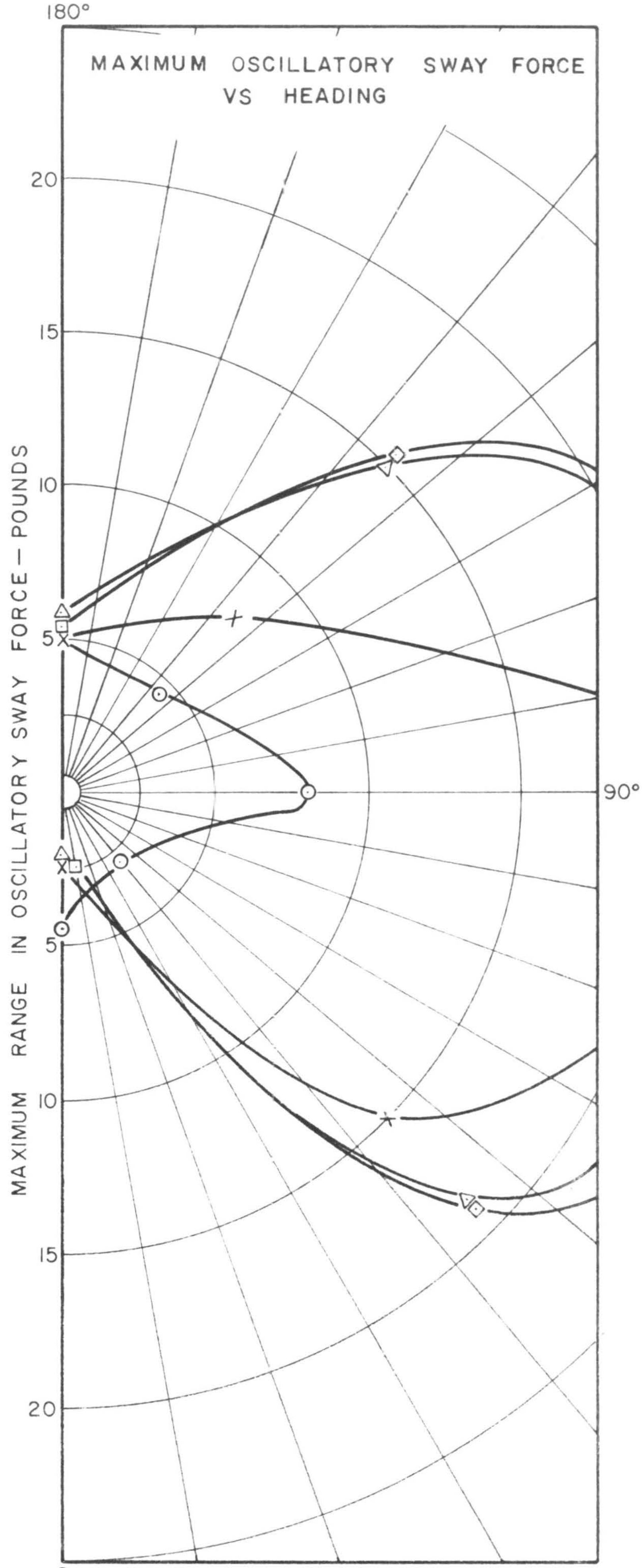

MAXIMUM OSCILLATORY SWAY FORCE VS HEADING
MAXIMUM RANGE IN OSCILLATORY SWAY FORCE — POUNDS
180°
20
15
10
5
5
10
15
20
0
90°

FIG. 37

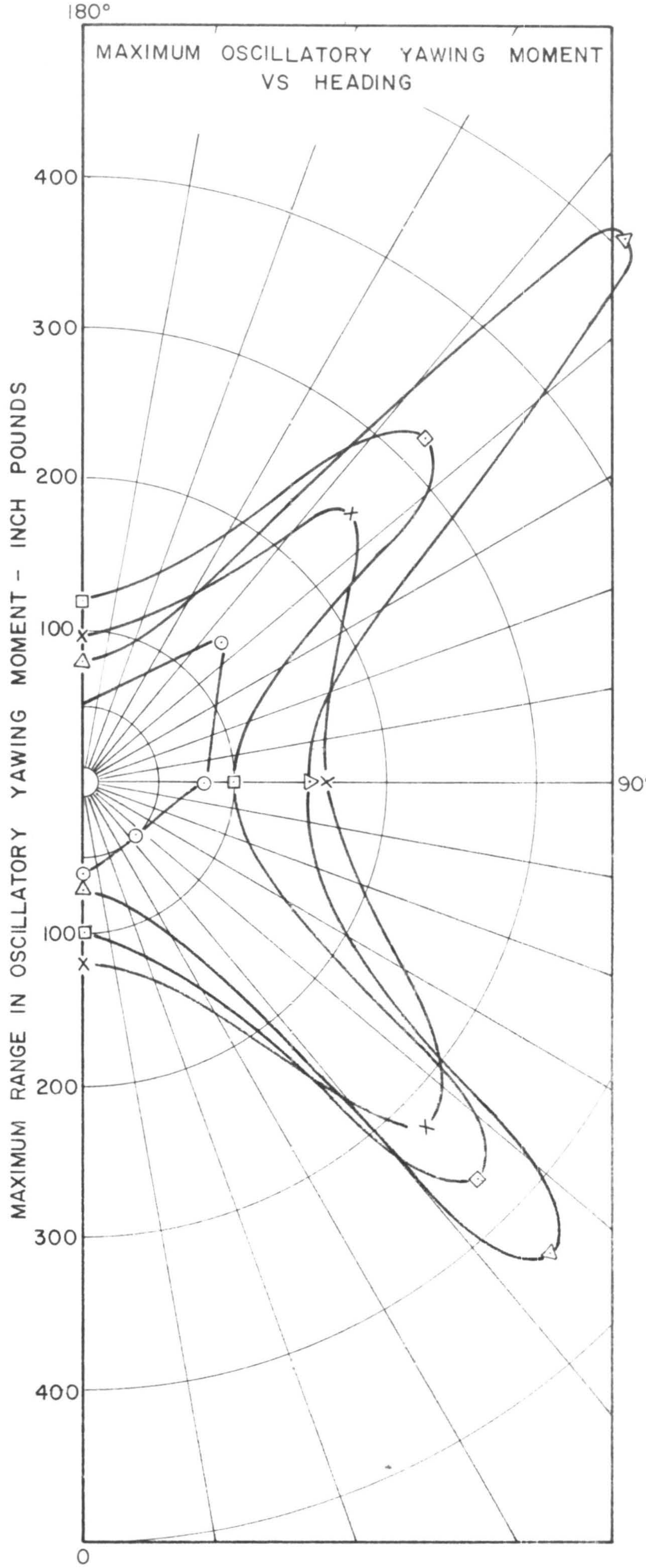

180°
MAXIMUM OSCILLATORY YAWING MOMENT
VS HEADING
400
300
200
100
100
200
300
400
90°
0
MAXIMUM RANGE IN OSCILLATORY YAWING MOMENT - INCH POUNDS

FIG. 38

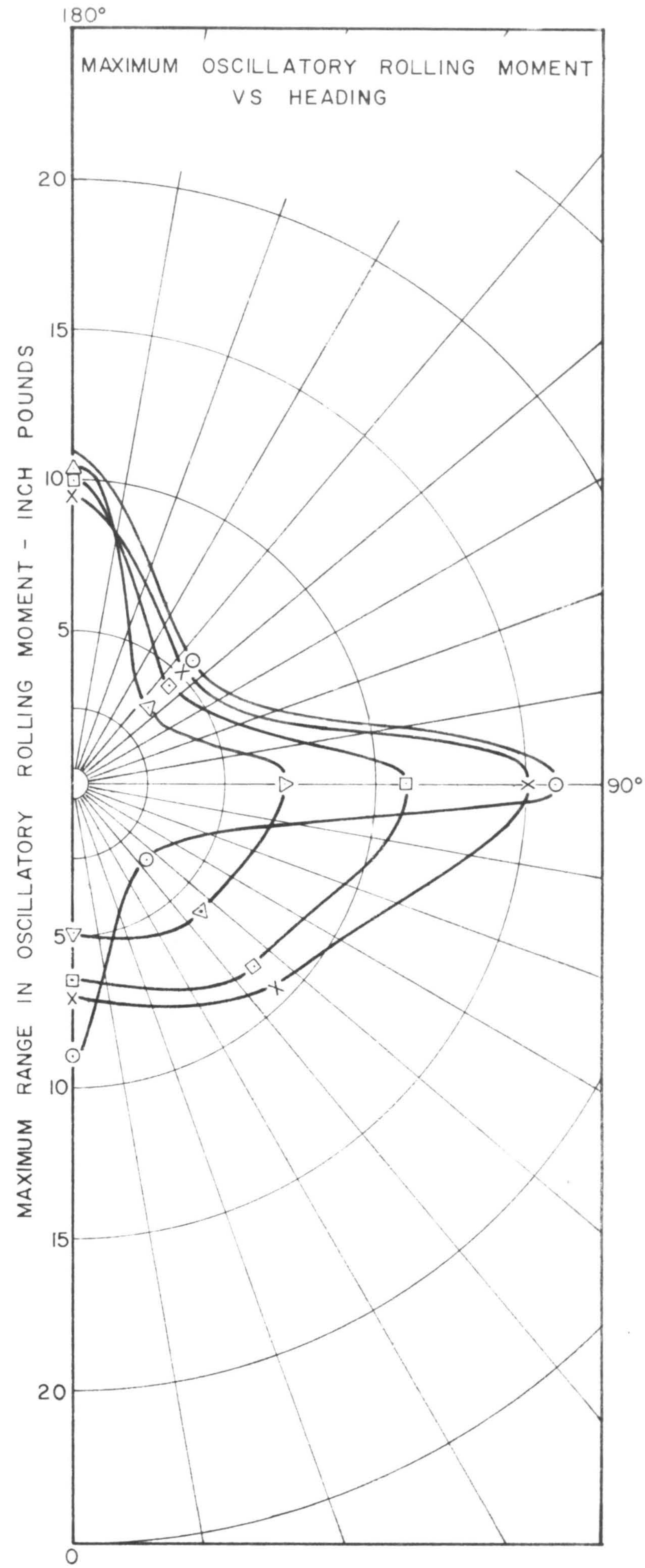

MAXIMUM OSCILLATORY ROLLING MOMENT
VS HEADING
MAXIMUM RANGE IN OSCILLATORY ROLLING MOMENT - INCH POUNDS
180°
90°
0
5
10
15
20

FIG. 39

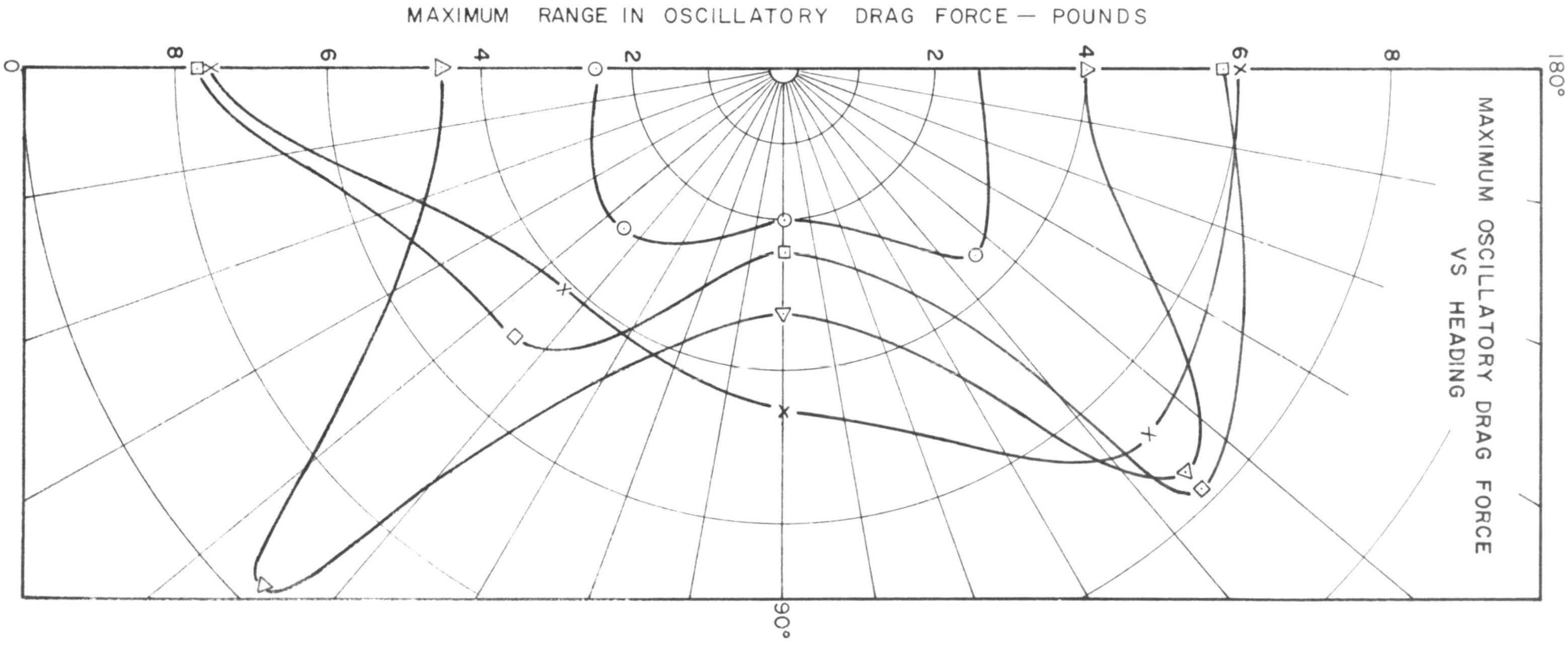

MAXIMUM OSCILLATORY DRAG FORCE
VS HEADING

FIG. 40

Mailing List for Final Report Contract Nonr 1610(04)

No. of Copies	
75	David Taylor Model Basin Department of the Navy Washington 7, D. C. Attention: Code 513
1	Office of Naval Research Resident Representative 108 Malott Hall Lawrence, Kansas
1	Office of Naval Research Chicago Branch Office John Crevar Library Bldg. 86 East Randolph Street Chicago 1, Illinois
1	Office of Naval Research New York Branch Office 346 Broadway New York 13, New York
1	Office of Naval Research San Francisco Branch Office 1000 Geary Street San Francisco 9, California
4 (1 to each Code No.)	Chief, Bureau of Ships Department of the Navy Washington 25, D. C. Attention: Codes 335, 420, 440
3	University of California Department of Naval Architecture Berkeley 4, California Attention: Professor H. A. Schade
2	Massachusetts Institute of Technology Department of Naval Architecture and Marine Engineering Cambridge 39, Massachusetts Attention: Professor M. A. Abkowitz

Mailing list for final report continued (Contract Nonr 1610(04)

No. of Copies	
2	University of Michigan Department of Naval Architecture Ann Arbor, Michigan Attention: Professor R. B. Couch
2	Stevens Institute of Technology Davidson Laboratory 711 Hudson Street Hoboken, New Jersey Attention: Dr. J. P. Breslin, Director
4	Chief of Naval Research Department of the Navy Washington 25, D. C. Attention: Code 438
1	Commanding Officer Office of Naval Research Branch Office 495 Summer Street Boston 10, Massachusetts
1	Commanding Officer Office of Naval Research Branch Office 1030 East Green Street Pasadena 1, California